J. Fluid Mech. (1983), *vol.* 137, *pp.* 83–113
Printed in Great Britain

Structure of a turbulent separation bubble

By MASARU KIYA AND KYURO SASAKI
Faculty of Engineering, Hokkaido University, Sapporo, 060, Japan

(Received 12 January 1983 and in revised form 6 July 1983)

Flow in the separation bubble formed along the sides of a blunt flat plate with right-angled corners has been studied in terms of extensive single- and two-point measurements of velocity and surface-pressure fluctuations. The cross-correlations between the surface-pressure and velocity fluctuations are found to be useful for the study of large-scale vortex structure in the bubble. Large-scale vortices are shed downstream from the separation bubble with a frequency of about $0.6U_\infty/x_R$, where U_∞ is the approaching velocity and x_R is the time-mean length of the bubble. On top of this regular vortex shedding, there exists a large-scale unsteadiness in the bubble. Vortices which are much larger than the regular vortices are shed with frequencies less than about $0.2U_\infty/x_R$. The large-scale unsteadiness is accompanied by enlargement and shrinkage of the bubble and also by a flapping motion of the shear layer near the separation line. The intermittent nature of the flow in the bubble is clarified in some detail. The distributions of the cross-correlations between the pressure and velocity fluctuations demonstrate the vortex structure in the reattaching zone. The longitudinal distance between the vortices is estimated to be $(0.7–0.8)x_R$ and their convection velocity is about $0.5U_\infty$ near the reattachment line. The cross-correlations also suggest the existence of a longitudinal counter-rotating system in the bubble. The distance between the axes of the rotation is of the order of $0.6x_R$. Variations of timescales, lengthscales and phase velocities of the vortices are presented and discussed.

1. Introduction

Flows at high Reynolds number with separation and reattachment have long been a subject of many studies. Reviews on these flows, together with lists of references, are included in articles by Fernholz (1978) and Johnston (1978). In this paper, we are concerned with a two-dimensional separation–reattachment flow (hereinafter called a 'separation bubble') where the separation occurs from a sharp corner. An excellent critical review of previous studies in this category is given by Bradshaw & Wong (1972).

Very little is still known of details of the flow structure in the reattaching zone where the separated shear layer reattaches onto a solid surface. A fundamental work in this direction is Wood & Bradshaw's (1982) experimental study of a turbulent plane mixing layer constrained by a solid surface. The behaviour of large-scale vortices in the reattaching zone plays a decisive role in determining flow properties not only in the separation bubble but in the developing region downstream of the bubble. An extensive measurement of turbulence in the developing region downstream of a downward-facing step is reported by Chandrsuda & Bradshaw (1981). Bradshaw & Wong (1972) argue that the large vortices are torn virtually into two in the reattaching zone and that there is thus an abrupt change in the lengthscales of the

vortices. To the best of our knowledge, however, such changes in lengthscales have not yet been confirmed experimentally.

We consider in this paper a separation bubble formed along a side of a blunt flat plate with right-angled corners (figure 1). The plate is aligned in such a way that the sides are parallel to an approaching uniform flow. The plate is long enough for the interaction between the separation bubbles on both sides to be negligible, so that attention can be confined to one of the separation bubbles. This particular separation bubble was chosen in this study in view of the following reasons.

(i) The thickness δ of the boundary layer on the separation line is much smaller than the height $2H$ of the plate when the Reynolds number is sufficiently high. The thin shear layer enables us to omit the parameter $\delta/2H$ from the interpretation of the experimental results.

(ii) The solid surface downstream of the separation line belongs to one of the simplest shapes. Since the shape of an afterbody affects the separation bubble, it should be as simple as possible in order to obtain essential features of the bubble.

The time-mean velocity and pressure, turbulence intensities and Reynolds shear stress in this separation bubble are reported by several authors (Ota & Itasaka 1976; Ota & Narita 1978; Kiya, Sasaki & Arie 1982, hereinafter referred to as KSA). Measurements are also made of the r.m.s. value, power spectrum, integral timescale and cross-correlation between the surface-pressure and velocity fluctuations (Hillier & Cherry 1981*a*, *b*; KSA). The last reference is mainly addressed to a discrete-vortex simulation of the separation bubble. Observations of vortices in the bubble are reported at low and moderate Reynolds numbers by Lane & Loehrke (1978) and Ota, Asano & Okawa (1981).

Hillier & Cherry (1981*a*) showed the existence of a low-frequency unsteadiness in the separation bubble, some of its basic phenomena, the shedding of vortical structure from the reattaching region, and the fact that the unsteady motion is significantly three-dimensional. In the present paper, these features are confirmed and extended by more detailed measurements. The low-frequency unsteadiness is also observed in the separation bubble behind a downward-facing step (Eaton & Johnston 1982). They suggest that the likely cause of the low-frequency motion is an instantaneous imbalance between the entrainment rate from the recirculation zone and the reinjection near the reattachment line.

The information obtained from the abovementioned studies, however, is not adequate enough to clarify the structure of large eddies in the separation bubble, especially in the reattaching zone. A good deal of work is needed to understand the separation-bubble flows well enough to predict their behaviour in general. The purpose of this paper is to present some new measurements which demonstrate the phenomenon of the separated shear layer and the structure of large-scale vortices in the bubble more clearly than the previous studies. The velocity and surface-pressure fluctuations and their cross-correlations were extensively measured in the separation bubble. The pressure fluctuations along the surface of the plate were found to be indicative of the large-scale vortices, so that they were used as reference signals to sort out the velocity fields associated with the vortices. The velocity–pressure correlations were utilized to find coherent vortices in turbulent boundary layers (Willmarth & Wooldridge 1963).

Figure 1 shows the definition of symbols. The Cartesian coordinates x, y, z are defined in such a way that the x-axis is in the longitudinal direction, the y-axis is vertically outwards from the side, and the z-axis is normal to the x- and y-axes so as to form a right-handed system. The origin is located at an edge of the plate whose

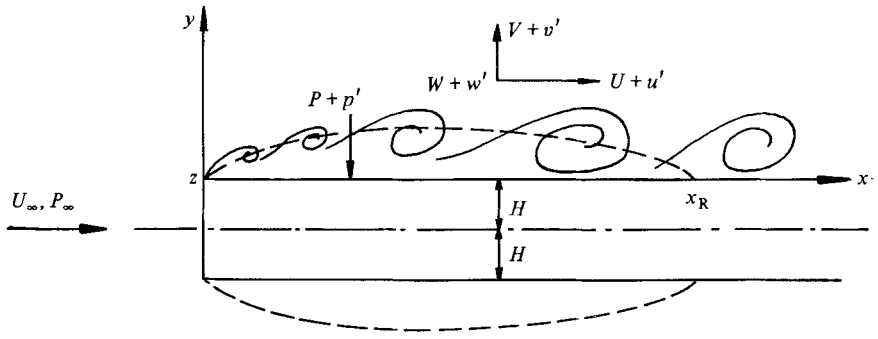

FIGURE 1. Configuration of flow and definition of symbols.

thickness is denoted by $2H$. The time-mean components of velocity in the x-, y-, z-directions and surface pressure are denoted by U, V, W and P respectively, and the corresponding fluctuating components by u', v', w' and p'. The root-mean-square values of the fluctuating quantities will be denoted by the suffix rms. Since the time-mean flow is in the (x, y)-plane, the velocity component W is practically zero. The velocity at infinity upstream is denoted by U_∞ and the pressure there by P_∞. The time-mean reattachment line is written as x_R.

In §2 the experimental apparatus is briefly discussed. In §3 the results are presented and discussed. Finally a summary of the results is given in §4.

2. Experimental apparatus and methods

Experimental apparatus and method will be only briefly described here because they were mostly the same as those employed in KSA. Experiments were performed in an open-return low-speed air tunnel with a working section 40 cm high, 20 cm wide and 1 m long. The freestream turbulence, which was originally 0.4 %, was reduced to 0.2 % at the speed of 20 m/s by enclosing the intake of the tunnel by glass-wool screens. The reduced freestream turbulence yielded a 5 % longer separation bubble than in KSA.

The blunt plate tested was 2 cm thick, 50 cm long and 20 cm wide. Its leading edge was right-angled and located 50 cm downstream of the beginning of the test section. The plate spanned the tunnel horizontally along its centreline, thus having an aspect ratio of 10. No endplates were used. A number of pressure taps of 0.7 mm diameter were fitted along the lower side of the plate at the midspan. An exact alignment of the plate was found by matching pressures recorded on tappings located at the upper and lower surfaces of the plate 5.5, 11.0 and 27.0 cm from the leading edge.

The Reynolds number was based on the freestream velocity and the height of the plate was 2.6×10^4 throughout the present experiment.

The tunnel-wall blockage, which originally amounted to 5 %, was corrected by fitting false boundaries along the ceiling and floor of the test section. The false boundaries were curved according to the blockage-free streamline, flared by an amount equal to the displacement thickness of the boundary layer along the tunnel walls, and joined smoothly to the bell entrance of the test section.

The time-mean and fluctuating velocities were measured by linearized constant-temperature hot-wire anemometers using single and X-wire probes and split-film probes. The hot wires were tungsten wires of 5 μm diameter with a working length

of about 1 mm. The X-wires were inclined by $\pm 45°$ with respect to the main-flow direction. The hot wires were calibrated statically in the undisturbed part of the flow in the test section by assuming a cosine-law response to yaw. The overheat ratio of the hot wires was about 1.5. Square-wave tests showed the maximum frequency response to be about 10 kHz. No corrections were made for the effects of high turbulence intensities on the time-mean and fluctuating velocities except when otherwise stated.

Two kinds of split-film sensors of diameter 0.132 mm (produced by Thermo-Systems Inc.) were employed. One had the plane of the split normal to the main flow, and thus was able to detect reversals of the local flow direction. This was used to measure U, u' and the reverse-flow intermittency in the whole region of the bubble. The other, which had the plane of the split parallel to the main flow, was used to measure u' and v' in regions where the reverse-flow intermittency was lower than 0.1. In regions of high turbulence with low time-mean velocity, u' fluctuations measured by the former are more reliable than those measured by the hot-wire probes. The split-film sensors were calibrated statically in the undisturbed flow according to *Technical Bulletin* TB20 *TSI Split Film Sensor Calibration and Applications* in a slightly modified manner. A response of the split-film probes was checked by comparing measured u' spectra with those obtained by the single hot-wire probe in a grid turbulence of $u'_{\rm rms}/U_\infty = 0.058$ and $U_\infty = 10$ m/s. The spectra were practically identical for frequencies less than about 1.5 kHz, the energy in high frequencies being higher for the hot wire than for the split films.

Hot-wire results of velocity are likely to be reliable only if the ratio $u'_{\rm rms}/U$, say, is less than about 0.3, while if the relative intensity exceeds 0.5 hot-wire results are likely to be highly unreliable (Chandrsuda & Bradshaw 1981). Results within the band of $0.3 < u'_{\rm rms}/U < 0.5$ should thus be treated with caution.

The hot-wire and split-film probes were mounted on a traversing mechanism outside the tunnel. This allowed the positioning of the probe to be adjusted with an accuracy of 0.1 mm. Pressure fluctuation on the plate surface was detected by a semiconductor strain-gauged transducer, which was mounted inside the plate with a small cavity between a pressure tap of 0.7 mm diameter and the diaphragm of the transducer. The gain factor of the transducer was 1 ± 0.06 up to 530 Hz, with negligibly small phase shift. Most of the measurements were made in the midspan plane.

The velocity and pressure fluctuations were recorded on two or three channels of an analogue tape recorder and later analysed by a computer (HITAC M200) or a digital signal processor (SANEI 7T07A) to obtain various statistical properties. No sensible phase lag was found to exist between the pressure transducer and the hot-wire anemometers and between the hot-wire anemometers.

The flow was called 'turbulent' and the intermittency function was set to unity if the short-time averaged energy

$$\widetilde{u'^2_{\rm T}} = \frac{1}{\Delta t}\int_{t-\frac{1}{2}\Delta t}^{t+\frac{1}{2}\Delta t} u'^2_{\rm T}(t)\,{\rm d}t,$$

was greater than a threshold value. Here $u'_{\rm T}$ was obtained by high-pass filtering (4 kHz) the longitudinal velocity fluctuation u'. The cut-off frequency 4 kHz was chosen because the dissipation spectrum $f^2E_{u'}(f)$ attained a maximum approximately at this frequency. It is reasonable to assume that the flow is turbulent in regions where this high-frequency fluctuation is detected. The high-frequency fluctuation has small amplitudes so that $u'^2_{\rm T}$ is not influenced markedly in character by reversals of the flow

direction. The time interval Δt of the integration was chosen to be 0.8 ms, which is about one-tenth of the vortex-shedding period (see §3.3). The threshold value was selected as $3 \times 10^{-5} U_\infty^2$ by comparing simultaneously the waveforms of $u_T'^2$ and the intermittency function. The high-frequency energy in the potential field was assumed to be well below the threshold level. This method of obtaining the intermittency function is similar to that of Fiedler & Head (1966).

Fluid in the separation bubble moves intermittently back and forth corresponding to the formation and subsequent downstream shedding of large-scale vortices. The fraction of time during which the flow is in the upstream direction is defined as the reverse-flow intermittency I_r. Measurements of I_r were made by the split-film probe. The split-film output $u(t)$ was averaged during a short time interval Δt, i.e.

$$\tilde{u}(t) = \frac{1}{\Delta t} \int_{t-\frac{1}{2}\Delta t}^{t+\frac{1}{2}\Delta t} u(t)\, \mathrm{d}t,$$

where Δt was chosen to be 0.8 ms. The signal $\tilde{u}(t)$ was subsequently used to calculate I_r.

3. Results and discussion

3.1. *Two-dimensionality of the flow and the end effects*

As mentioned in §2, no endplates were employed in this experiment. One may argue that the endplates should be used to improve the two-dimensionality by modifying the flow in the junction between the tunnel wall and the plate. It should be noted, however, that the use of the endplates cannot necessarily suppress a vortex system in the junction, i.e. a horseshoe vortex and longitudinal trailing vortices. Hillier & Cherry (1981*a*) correctly state that the endplates are unlikely to improve the two-dimensionality of the unsteady flow field in the separation bubble. The use of the endplates cannot be regarded as compulsory.

The spanwise uniformity of the time-mean and r.m.s. longitudinal velocities was checked in the time-mean reattachment section, where the flow was suspected to be most disturbed by the end effects. The uniformity was found to be excellent over a region $\pm 3.5H$ on both sides of the midspan, the maximum variations in U and u'_{rms} in this section being less than 1.5% and 1% respectively of the freestream velocity. In regions $|z/H| \gtrsim 4.0$, however, the two-dimensionality decreased as $|z/H|$ increased. The surface-flow visualization (see figure 9 of KSA) showed a fairly two-dimensional pattern in the region $|z/H| \lesssim 4$. This extent of the spanwise uniformity was conjectured to be tolerably large to ensure that the separation-bubble properties which were measured in the midspan plane were representative of the infinite-span case. The present aspect ratio of 10 is partially justified by the fact that the reduction of the aspect ratio of 13.2–9.33 produces no systematic effect on the bubble length or mean and fluctuating quantities (Hillier & Cherry 1981*a*). Some features of the separation bubble to be presented in the following are possibly contaminated to a certain extent by the vortex system in the junction. We feel that such contamination is not serious, because, as will be demonstrated later, some of the present results do agree with Hillier & Cherry's (1981*a*) data taken at the aspect ratio of 13.2, which they claim to be sufficiently large. The vortex system is supposed to be fairly steady, so that it is unlikely to produce significant fluctuating quantities in the separation bubble.

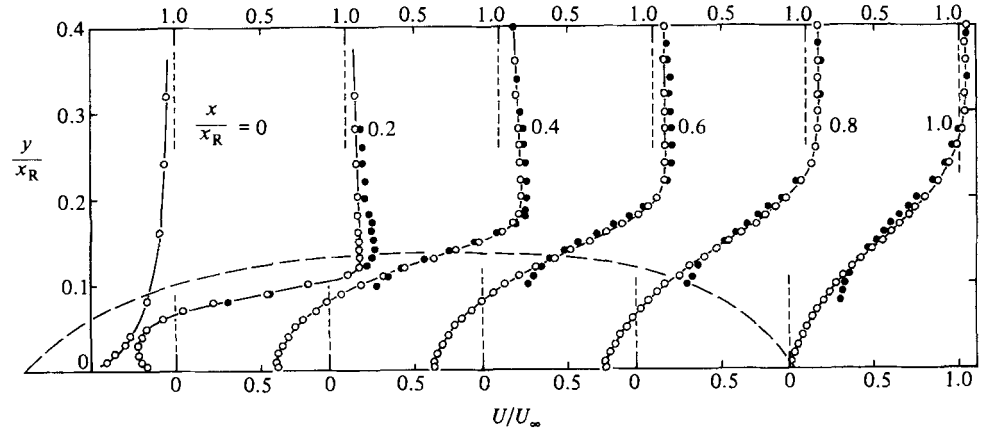

FIGURE 2. Distribution of time-mean longitudinal velocity in and around the separation bubble: ○, split-film result; ●, X-wire result corrected for high turbulence intensities; ——, dividing streamline (solid lines for visual aid only).

3.2. *Mean-flow properties*

The time-mean reattachment line of the separated shear layer was found to be at $x/H = 10.1$ on the basis of the reverse-flow intermittency (see figure 10), i.e. $x_R = 10.1H$. Profiles of the longitudinal mean velocity U measured by the split-film probe are shown in figure 2, together with those obtained by the X-wire probe. The hot-wire results were corrected for the effect of high turbulence intensities by noting that the addition of time-mean outputs of the X-wire probes yields

$$2^{\frac{1}{2}}U(1 + w'^2_{\rm rms}/U^2 + \text{higher-order terms}).$$

The term $w'^2_{\rm rms}/U^2$ was corrected by iteration in terms of measured $w'^2_{\rm rms}$. The hot-wire results are seen to be reliable in regions where U/U_∞ is greater than about 0.4.

In order to show the development of the separated shear layer, it is convenient to introduce a few representative parameters. A position where $u'_{\rm rms}$ attains a maximum value can be interpreted as the centre of the shear layer because the lateral distributions of U have a point of inflexion in the vicinity of this position. The normal distance between this position and the plate surface is denoted by y_C. The time-mean edge of the shear layer y_δ was defined as a position where U amounts to 99% of a maximum velocity. Another edge y_B was defined as a position at which an intermittently turbulent signal first appeared when a hot-wire probe was traversed vertically from outside of the separation bubble. Although one may anticipate a considerable uncertainty in determining y_B, this position is believed to be obtained with the same accuracy as y_δ. The results are shown in figure 3. The position y_C changes only slightly in the region $x/x_R \geqslant 0.6$, where y_C/x_R is approximately equal to 0.14. The positions y_δ and y_B, on the other hand, continue to increase with increasing x approximately in proportion to $x^{\frac{1}{2}}$.

The time-mean surface pressure in the separation bubble was in fairly good agreement with the results of KSA and Hillier & Cherry (1981*b*).

3.3. *Velocity fluctuations*

Since distributions of the r.m.s. velocities $u'_{\rm rms}/U_\infty$ and $v'_{\rm rms}/U_\infty$ and the Reynolds shear stress $-\overline{u'v'}/U^2_\infty$ were generally the same as those given in KSA, only the

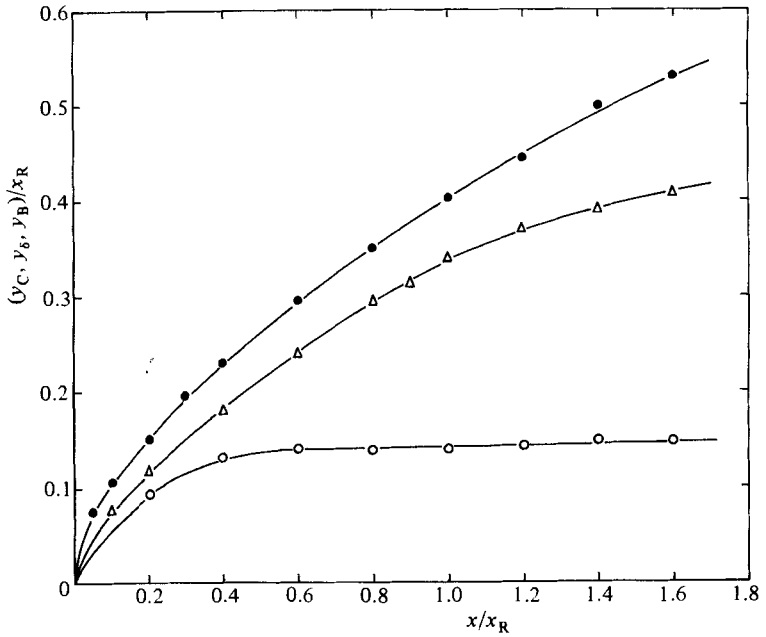

FIGURE 3. Three representative positions of the separation–reattachment flow: ○, y_C; △, y_δ; ●, y_B (solid lines for visual aid only).

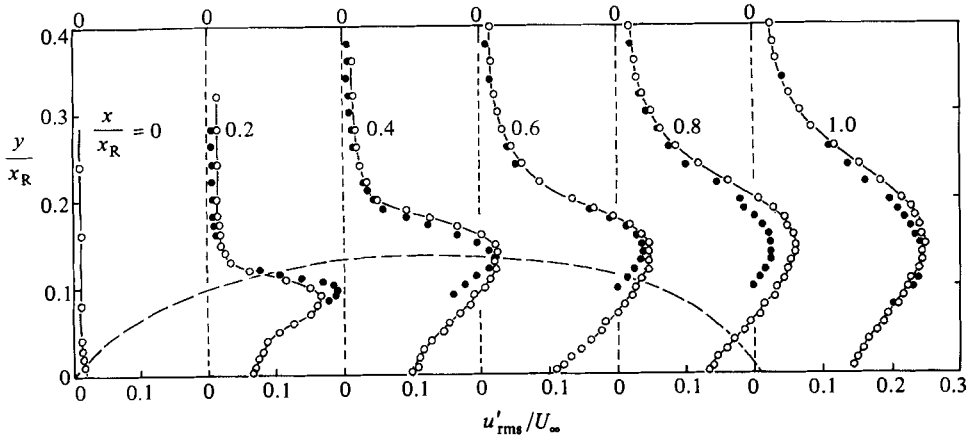

FIGURE 4. Distributions of r.m.s. longitudinal velocity u'_{rms}/U_∞: ○, split-film result; ●, X-wire result; ---, dividing streamline (solid lines for visual aid only).

split-film results will be presented. The transverse r.m.s. velocity w'_{rms}/U_∞ was also measured, but will not be presented.

The distributions of u'_{rms}/U_∞ are shown in figure 4, which compares two sets of data measured by the split-film and X-wire probes. They are in fairly good agreement in regions where $u'_{rms}/U_\infty \lesssim 0.5$. Figure 5 compares the lateral r.m.s. velocity v'_{rms}/U_∞ measured by the split-film probe with the X-wire result in the reattachment section $x/x_R = 1.0$. The latter is seen to be reliable only in the region $y/x_R \gtrsim 0.15$, where the reverse-flow intermittency (see §3.4) is zero.

In the neighbourhood of the dividing streamline, the level of the r.m.s. velocities

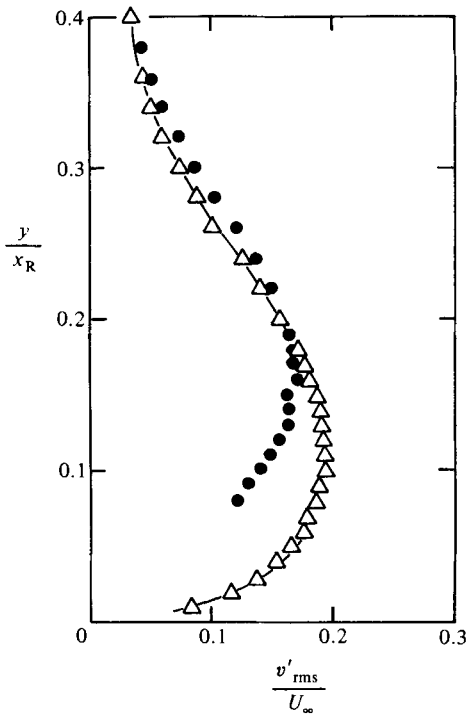

FIGURE 5. Distributions of r.m.s. lateral velocity v'_{rms}/U_∞ in the reattachment section $x/x_R = 1.0$: △, split-film result; ●, X-wire result (solid line for visual aid only).

were in the order u'_{rms}, w'_{rms} and v'_{rms}. This order is the same as that in the turbulent plane mixing layer between a uniform stream and a still fluid (Wygnanski & Fiedler 1970). Maximum values of u'_{rms}/U_∞, w'_{rms}/U_∞ and v'_{rms}/U_∞ were roughly 0.20, 0.20 and 0.13 respectively for $x/x_R \lesssim 0.4$, and 0.25, 0.22 and 0.17 for $x/x_R \gtrsim 0.6$, while the corresponding maximum r.m.s. velocities in the plane mixing layer are 0.18, 0.15 and 0.14 (Wygnanski & Fiedler 1970). Since the maximum velocity difference U_M in the longitudinal velocity component across the shear layer is larger than the freestream value U_∞, the comparison with the data of the plane mixing layer may be made more appropriately by employing U_M as a reference velocity than U_∞. The maximum values of u'_{rms}/U_M, w'_{rms}/U_M and v'_{rms}/U_M were on the average 0.14, 0.15 and 0.09 respectively for $x/x_R \lesssim 0.4$, and 0.21, 0.18 and 0.14 for $x/x_R \gtrsim 0.6$. The somewhat smaller values of the r.m.s. velocities in the upstream region $x/x_R \lesssim 0.4$ than in the plane mixing layer are possibly associated with the stabilizing effect of the convex curvature of the separated shear layer (Johnston 1978). Flow-visualization studies (Lane & Loehrke 1980; Ota *et al.* 1981) and the discrete-vortex simulation of KSA suggest that the rolled-up vortices in the shear layer contact with the surface roughly at $x/x_R = 0.5$; the behaviour of the large vortices and thus the velocity fluctuations in the region $x/x_R \gtrsim 0.5$ are possibly affected by the presence of the solid surface.

The Reynolds shear stress in the reattachment section $x/x_R = 1.0$ is shown in figure 6. The split-film result for the maximum value of $-\overline{u'v'}$ is larger by about 30% than the hot-wire result. Since the hot wire was aligned parallel to the plate surface, its result is probably affected by a relatively large longitudinal curvature of time-mean streamlines. The measured $-\overline{u'v'}$ is known to be sensitive to a small misalignment of the probe with respect to the inclination of the time-mean streamlines. The split-film

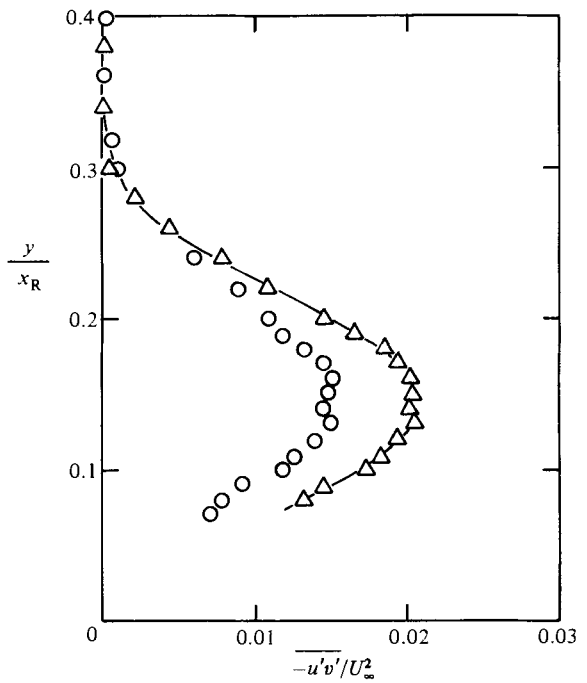

FIGURE 6. Distribution of Reynolds shear stress in the reattachment section $x/x_R = 1.0$: △, split-film result; ○, X-wire result (solid line for visual aid only).

data are supposed to be more reliable because this probe can detect the u' and v' fluctuations irrespective of the mean-flow inclinations in regions where the reverse-flow intermittency is zero.

Figure 7 shows the power spectrum $E_{u'}$ of u' together with the surface-pressure spectrum $E_{p'}$ in the reattachment section $x/x_R = 1.0$. The spectra are defined by

$$\int_0^\infty (E_{u'}, E_{p'})\, \mathrm{d}(fx_R/U_\infty) = (u'^2_{\mathrm{rms}}, p'^2_{\mathrm{rms}}),$$

where f is the frequency. The velocity spectrum at y_δ has a broad maximum at the frequency $fx_R/U_\infty \approx 0.6$, which is the same as the peak frequency of the surface-pressure spectrum. The disappearance of the peak at the centre y_C implies that the velocity fluctuations associated with large-scale coherent vortices were contaminated by those due to small-scale eddies. This suggests that the large-scale vortex structure in the separation bubble is reflected in the velocity fluctuations in the outer part of the bubble and in the surface-pressure fluctuations.

For a turbulent boundary layer with zero pressure gradient, Bradshaw (1967) shows that the peak frequency of the u' spectra in the irrotational field becomes lower as the distance from the turbulent region increases, and that the peak frequency tends to that of the surface-pressure spectrum as the hot-wire position approaches the edge of the turbulent region. Since these properties are believed to be independent of the turbulent structure, the u' spectra in the present case probably depend on the distance from the turbulent region. The velocity fluctuations in the irrotational field are driven by the large-scale vortices: it is reasonable to assume that the longitudinal motion of the large vortices is well reflected in the u' spectra near the edge of the turbulent region. This is the reason why the spectra were not measured beyond y_δ.

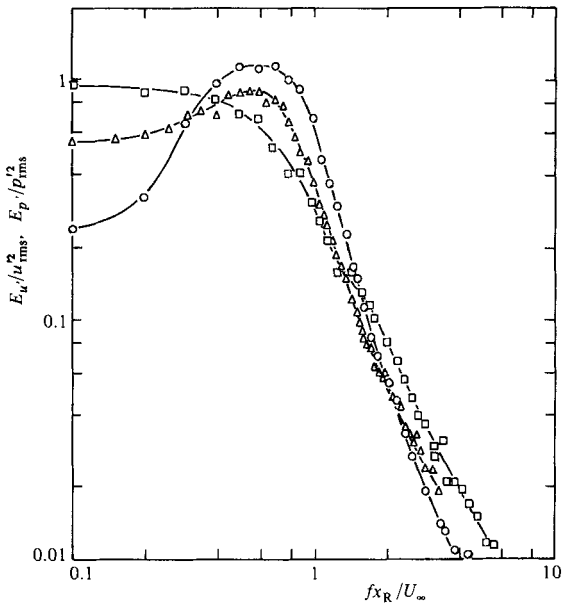

FIGURE 7. Power spectra of longitudinal-velocity and surface-pressure fluctuations in the reattachment section $x/x_{\rm R} = 1.0$: ○, $E_{u'}/u'^2_{\rm rms}$ at y_δ; □, $E_{u'}/u'^2_{\rm rms}$ at $y_{\rm C}$; △, $E_{p'}/p'^2_{\rm rms}$. Velocity fluctuations were detected by a single hot wire. (Solid lines for visual aid only.)

By the use of the unsteady form of Bernoulli equation and Taylor's hypothesis, Bradshaw (1967) demonstrates that in the potential field the pressure-fluctuation spectrum is nearly the same shape as the u' spectrum. He also argues that the low-frequency contributions to the pressure fluctuation could not differ markedly in character between the irrotational field and the surface, so that the surface-pressure spectrum has nearly the same shape as the u' spectrum near the edge of the turbulent region. The low-frequency range well includes the peak frequencies. A similarity in the u' spectrum at y_δ and the surface-pressure spectrum (figure 7) may suggest that Bradshaw's argument also applies to this more complex flow.

The cross-spectrum $|E_{u'v'}|$ and the phase $\phi_{u'v'}$ of the velocity fluctuations u', v' measured at the positions y_δ and $y_{\rm C}$ in the reattachment section are shown in figure 8. The cross-spectra attain a maximum at the frequency $fx_{\rm R}/U_\infty \approx 0.5$, which is near to the peak frequency of $E_{u'}$ and $E_{p'}$. It is reasonable to assume that these peaks of the spectra correspond to the shedding of large-scale vortices from the separation bubble. Such vortices are clearly observed in flow-visualization studies (Hillier & Cherry 1981*b*; Ota *et al.* 1981). From figures 7 and 8 and from the cross-spectra and coherence of surface-pressure and velocity fluctuations (figure 29), the typical vortex-shedding frequency is estimated to be $0.6U_\infty/x_{\rm R}$. This agrees fairly well with the value $0.7U_\infty/x_{\rm R}$ obtained by Hillier & Cherry (1981*a*). An examination of Eaton & Johnston's (1982) results for a separation bubble downstream of a two-dimensional sudden expansion, the expansion ratio being 3:5, reveals that the u' spectra in the reattaching zone have a broad but clear peak at a frequency $fx_{\rm R}/U_\infty = 0.5$, where U_∞ is taken as the main-flow velocity upstream of the expansion. The aspect ratio in their study is 12. The peak frequency is close to that for the leading-edge separation bubble. This feature strongly suggests a universal nature of two-dimensional separation bubbles downstream of a sharp corner.

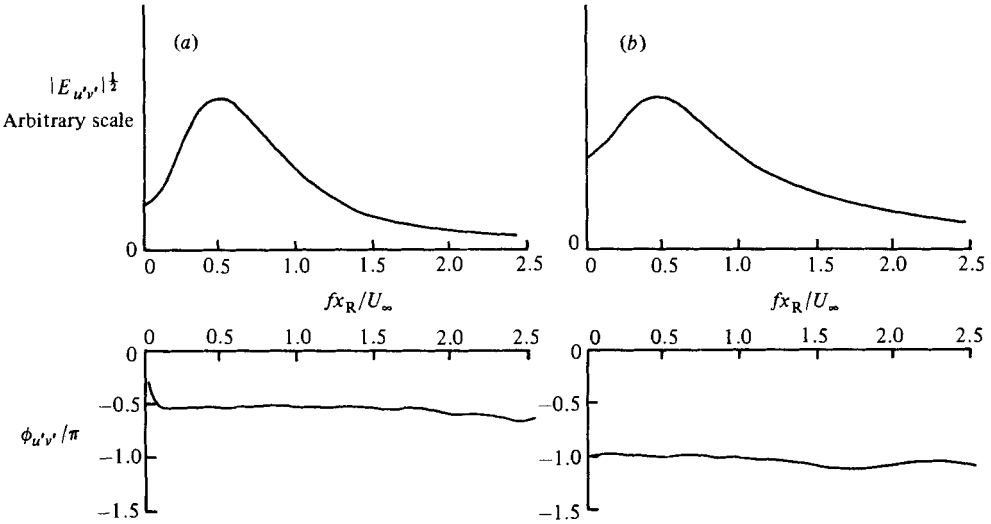

FIGURE 8. Cross-spectrum $|E_{u'v'}|$ and phase $\phi_{u'v'}$ of the velocity fluctuations u', v' in the reattachment section $x/x_R = 1.0$: (*a*) $y = y_\delta$; (*b*) $y = y_C$. Velocity fluctuations were detected by a X-wire probe. The vertical scales for $|E_{u'v'}|^{\frac{1}{2}}$ are linear but arbitrary.

It should be noted in passing that the phase $\phi_{u'v'}$ is about $\frac{1}{2}\pi$ and $-\pi$ at y_δ and y_C respectively. This is consistent with the fact that the velocity fluctuations u', v' at y_δ contribute very little to the Reynolds shear stress $-\overline{u'v'}$, while those at y_C produce the Reynolds shear stress most effectively at the frequency $fx_R/U_\infty \approx 0.5$.

Figure 9 shows the intermittency factor of turbulence γ_t plotted against the normalized distance y/y_δ, together with the result for the downward-facing step (Chandrsuda & Bradshaw 1981). The results are similar for the two cases, except that the maximum of γ_t is somewhat higher in the present case than in the downward-facing step. It is also interesting to note that γ_t never attains to unity through the reattachment section and that γ_t significantly decreases towards the wall.

The burst frequency f_t was defined as the number of turbulent bursts per unit time: f_t is zero if the flow at a fixed point is always laminar or turbulent. This was determined in terms of the intermittency function mentioned above. As shown in figure 9, the burst frequency becomes a maximum at the height where $\gamma_t = 0.5$, and, unlike turbulent boundary layers, increases towards the wall. These features suggest an intimate connection between flows in the outer and inner parts of the reattaching zone.

3.4. *Reverse-flow intermittency*

Figure 10 shows the longitudinal distribution of I_r measured at $y/x_R = 0.005$, together with the time-mean longitudinal velocity U_s at the same height. The position of $I_r = 0.5$ coincides exactly with that of $U_s = 0$. The time-mean reattachment line of the shear layer can be defined as the line where $I_r = 0.5$. It is interesting to note that I_r never becomes unity, even in the middle of the bubble. A sharp decrease of I_r towards the edge of the plate suggests the formation of a secondary separation bubble in the downstream vicinity of the separation line. These features of I_r are well represented by the discrete-vortex simulation of KSA. If the reattaching zone is defined rather arbitrarily as a region of $0.1 \leqslant I_r \leqslant 0.9$, its width is about $0.4x_R$.

The distribution of the intermittency across the separation bubble is shown in figure 11. The intermittency seems to attain a maximum near the plate surface.

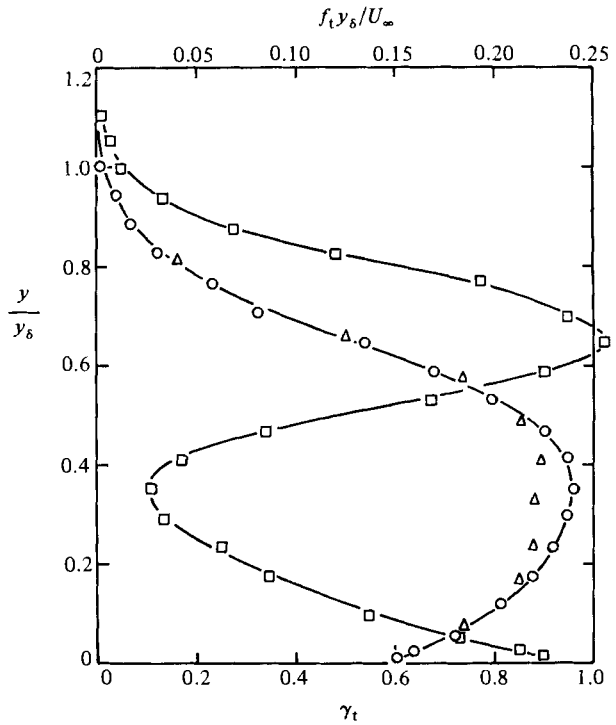

FIGURE 9. Turbulence intermittency factor γ_t and burst frequency f_t in the reattachment section $x/x_R = 1.0$: ○, γ_t (present result, hot-wire measurement); △, γ_t (Chandrsuda & Bradshaw 1981, downward-facing step); □, f_t (present result) (solid lines for visual aid only).

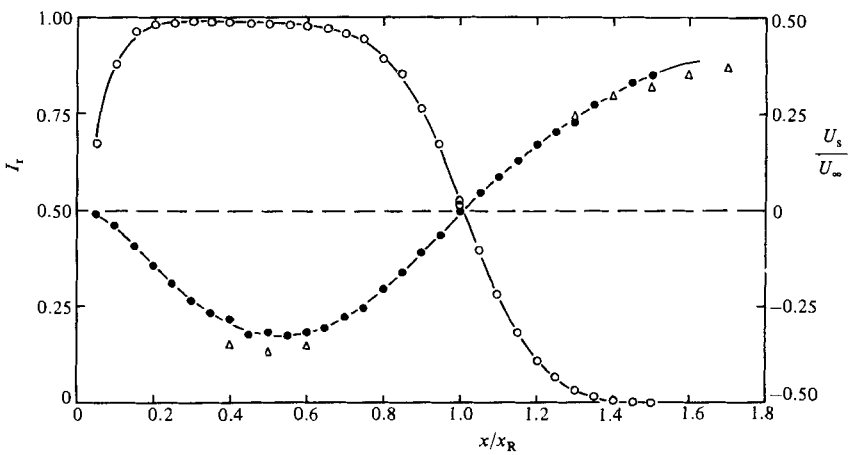

FIGURE 10. Distributions of reverse-flow intermittency I_r and time-mean longitudinal velocity U_s measured at the height $y/x_R = 0.005$: ○, I_r (split-film measurement); ●, U_s (split-film measurement); △, U_s (Pitot-tube measurement) (solid lines for visual aid only).

Figure 12 presents the distribution of the frequency f_r, which is half of the average number of changes in the flow direction during unit time: f_r is zero if the flow is always in one direction. The frequency f_r was obtained in terms of the short-time-averaged velocity $\tilde{u}(t)$. The non-dimensional frequency $f_r x_R/U_\infty$ takes a maximum value of about 0.7 along the line $I_r = 0.5$. This maximum value is not far from the frequency of vortex shedding from the separation bubble.

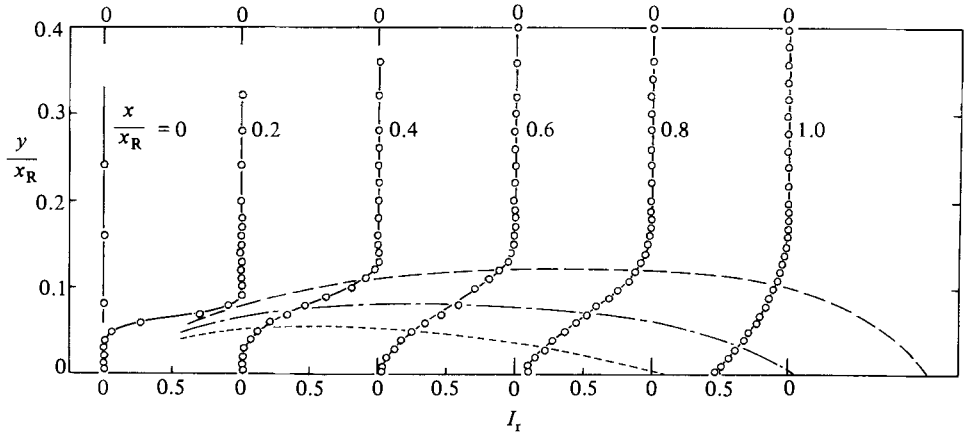

FIGURE 11. Distribution of reverse-flow intermittency I_r in the separation bubble; measurement by a split-film sensor: ——, $I_r = 0.1$; – – –, 0.5; - - - -, 0.9 (solid lines for visual aid only).

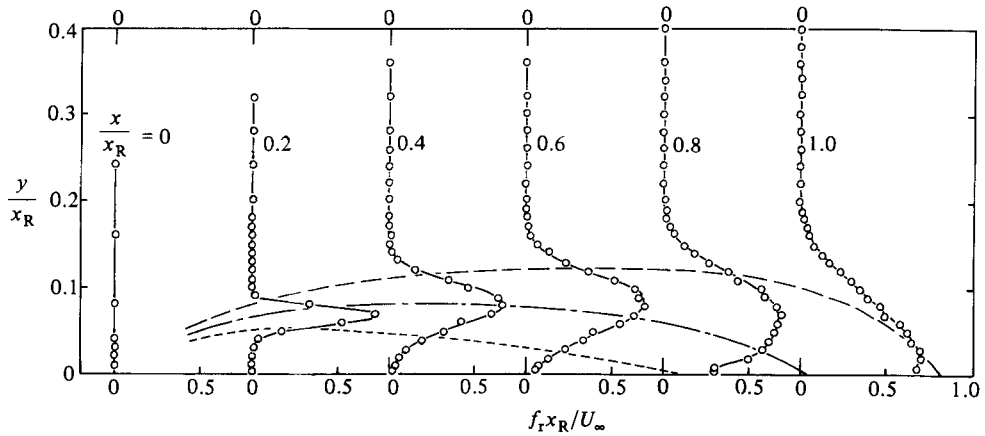

FIGURE 12. Distribution of frequency f_r, which is half of the average number of change in the flow direction during unit time; measurement by a split-film sensor: ——, $I_r = 0.1$; – – –, 0.5; - - - -, 0.9 (solid lines for visual aid only).

3.5. *Integral timescales of velocity fluctuations*

The integral timescales $T_{u'}$, $T_{v'}$ and $T_{w'}$ of the velocity fluctuations u', v' and w' respectively were obtained from the corresponding autocorrelation coefficients. Their distributions in the lateral direction are plotted in figure 13 for the reattachment section $x/x_R = 1.0$. The timescale $T_{u'}$ takes a minimum value in the vicinity of y_δ, whereas $T_{v'}$ and $T_{w'}$ are fairly constant in the region $y \leqslant \frac{1}{2}(y_\delta + y_C)$. The ratios $T_{u'}/T_{v'}$ and $T_{u'}/T_{w'}$ are roughly two in the inner region $y \lesssim y_C$ and roughly unity in the outer region $y \sim y_\delta$. Similar results were also obtained in the sections $x/x_R = 0.6$ and 1.4. Antonia & Van Atta (1977) observed the same feature in two-dimensional turbulent boundary layers.

Figure 14 shows the longitudinal distributions of the timescales $T_{u'}$, $T_{v'}$ and $T_{w'}$ measured at y_δ and denoted by $T_{u'\delta}$, $T_{v'\delta}$ and $T_{w'\delta}$ respectively. Also included is the timescale $T_{q'\delta}$ obtained by a single hot wire parallel to the z-axis. This timescale was presented in order to give a measure of the timescales near the separation line where the spatial resolution of the X-wire probes is poor owing to extremely small

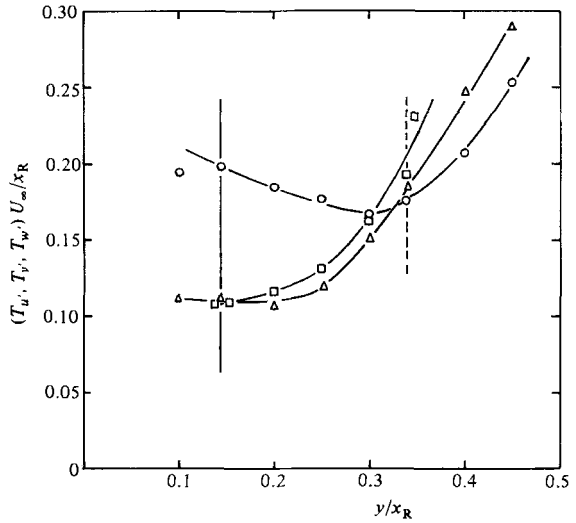

FIGURE 13. Distributions of integral timescales in the reattachment section. Measurement by X-wire probes: ○, $T_{u'}$; △, $T_{v'}$; □, $T_{w'}$. Vertical dotted and solid lines for y_δ and y_C respectively (other solid lines for visual aid only).

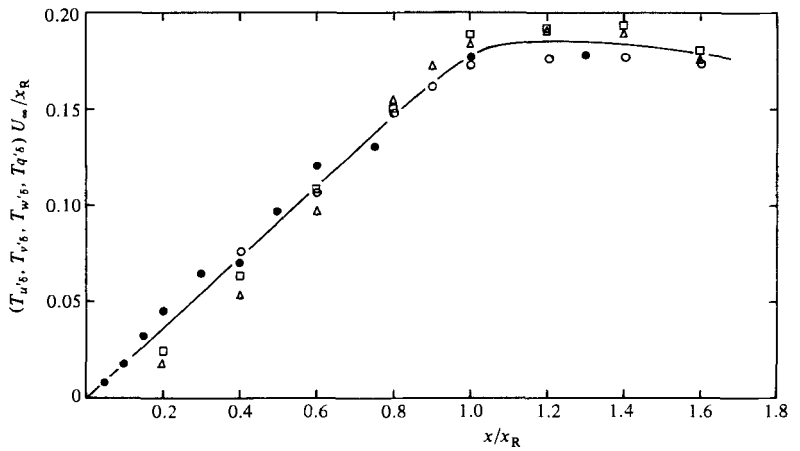

FIGURE 14. Change of integral timescales at y_δ in the longitudinal direction; measurement by single and X-wire probes: ○, $T_{u'\delta}$; △, $T_{v'\delta}$; □, $T_{w'\delta}$; ●, $T_{q'\delta}$ (solid line for visual aid only).

shear-layer thickness. The four timescales are roughly the same within the experimental uncertainties. They increase approximately linearly with increasing x up to the time-mean reattachment line, downstream of which the timescales are almost unchanged. An increase in the timescales can be interpreted as an increase in the size of coherent vortices under the assumption that the convection velocity of the vortices does not change significantly in the longitudinal direction. Nearly constant timescales downstream of the reattachment line are thus conjectured to result from hampered growth of the vortices due to the presence of the plate surface.

The timescales $T_{u'C}$, $T_{v'C}$ and $T_{w'C}$ of u', v' and w' respectively were also measured along the centre y_C (not presented here). The timescales $T_{v'C}$ and $T_{w'C}$ were almost the same and changed in the longitudinal direction in the same way as the timescales

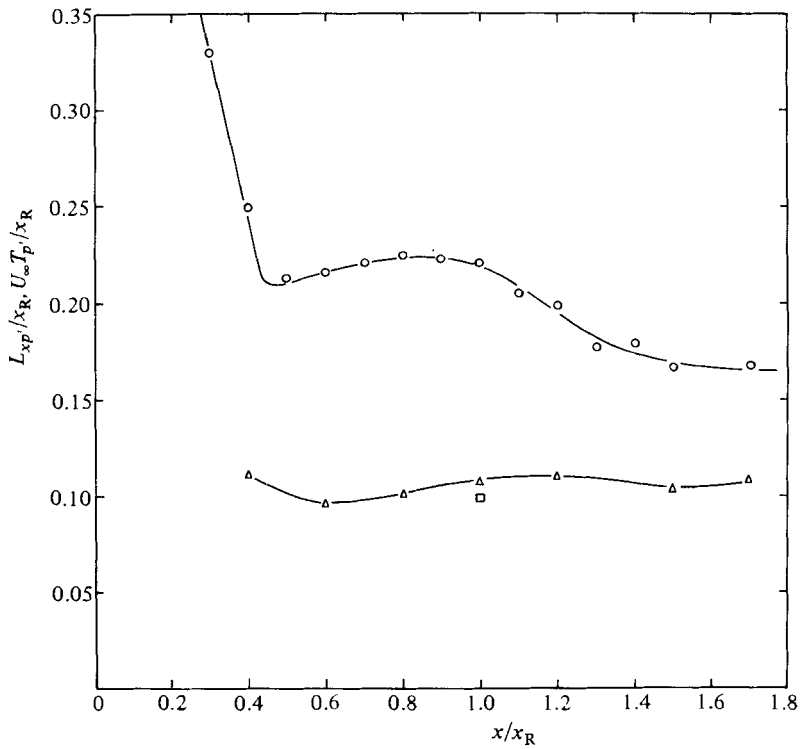

FIGURE 15. Integral timescale $T_{p'}$ and longitudinal lengthscale $L_{xp'}$ of surface-pressure fluctuation: ○, $T_{p'}$; △, $L_{xp'}$ (present result); □, $L_{xp'}$ (Hillier & Cherry 1981*a*) (solid lines for visual aid only).

at y_δ. The timescale $T_{u'C}$ was larger, very roughly by a factor of 2, than $T_{v'C}$ and $T_{w'C}$ in the vicinity and downstream of the reattachment line, whereas it was much larger than the latter near the separation line. This feature suggests that the u' velocity along y_C has contributions not only from the rolled-up vortices but also from another agent which had a much longer timescale than the vortices.

3.6. *Surface-pressure fluctuations*

The r.m.s. surface-pressure distribution was in fairly good agreement with the results of KSA and Hillier & Cherry (1981*b*). A broad maximum of about $0.12(\frac{1}{2}\rho U_\infty^2)$ appeared a little upstream of the reattachment line. The maximum was so broad that the r.m.s. pressure changed only insignificantly in the reattaching zone.

Figure 15 shows the integral timescale $T_{p'}$ of the pressure fluctuations plotted against the longitudinal distance. The timescale is fairly constant in the downstream half of the bubble, whereas in its upstream half $T_{p'}$ increases sharply towards the separation line. The latter feature is conjectured to be associated with a low-frequency lateral oscillation of the shear layer near the separation line, which will hereinafter be referred to as 'flapping' motion of the shear layer. The flapping is perhaps responsible for much larger $T_{u'C}$ than $T_{v'C}$ and $T_{w'C}$ shortly downstream of the separation line.

The timescale $T_{p'}$, together with the phase velocity $U_{cp'}$ of the pressure fluctuation, yields the longitudinal lengthscale $L_{xp'}(= U_{cp'} T_{p'})$. The result is also plotted in figure 15. The lengthscale has a fairly constant value of $0.11x_R$ from $x/x_R \approx 0.6$ to 1.7, which

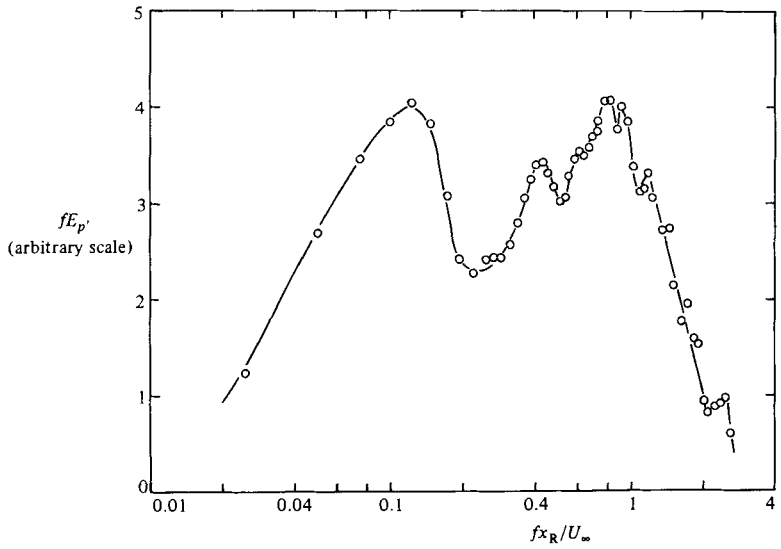

FIGURE 16. Surface-pressure spectrum $E_{p'}$ at the section $x/x_R = 0.2$; vertical scale is linear but arbitrary (solid line for visual aid only).

is the most distant section where the measurements were made. The value of $L_{xp'} = 0.11x_R$ is almost the same as the lengthscale $L_{xu'}$ of the longitudinal velocity fluctuation in the reattachment section (see figure 18). Accordingly it is reasonable to assume that the surface-pressure fluctuation is produced by the same large-scale vortices as those which are responsible for the velocity fluctuation u', at least in the vicinity of the reattachment section.

The pressure spectrum $E_{p'}$ at the reattachment section has been presented in figure 7. The peak frequency $fx_R/U_\infty \approx 0.6$ in figure 7 was also observed in the pressure spectra measured in the region $0.6 \leqslant x/x_R \leqslant 1.7$ and in Hillier & Cherry's (1981*a*) spectra in the range $0.55 \leqslant x/x_R \leqslant 1.35$. As shown in figure 16, the spectrum at $x/x_R = 0.2$ has a clear peak at $fx_R/U_\infty \approx 0.12$. The same peak frequency was observed at the position $x/x_R = 0.3$ (not given here). Moreover, the pressure spectra presented by Hillier & Cherry have a peak at the same frequency in the region $0.026 \leqslant x/x_R \leqslant 0.25$. As has been pointed out by Hillier & Cherry, this feature is a result of the flapping of the shear layer near the separation line, which will be described in detail in §3.8. Since the pressure spectrum in figure 16 takes a minimum at $fx_R/U_\infty \approx 0.2$, the flapping frequency is perhaps distributed in the range $fx_R/U_\infty \leqslant 0.2$, with a central frequency $fx_R/U_\infty = 0.12$.

In their downward-facing step flow, Eaton & Johnston (1982) observed a low-frequency unsteadiness which probably accompanies the flapping of the shear layer. Although the resolution of their u' spectra was not sufficient to identify any spectral peak in the low-frequency range, more than 30% of the measured u'^2_{rms} occurred at frequencies below $fx_R/U_\infty \approx 0.15$. This frequency is comparable to the central flapping frequency $fx_R/U_\infty = 0.12$ for the present case. Since the vortex systems in the ends of the plate are supposed to be markedly different from those in the ends of the expansion, almost the same value of the non-dimensional frequency suggests that the flapping is not directly connected to the flows in the ends.

The skewness of the surface-pressure fluctuation was positive in the reattaching zone, attaining a maximum near the reattachment line and being negative upstream

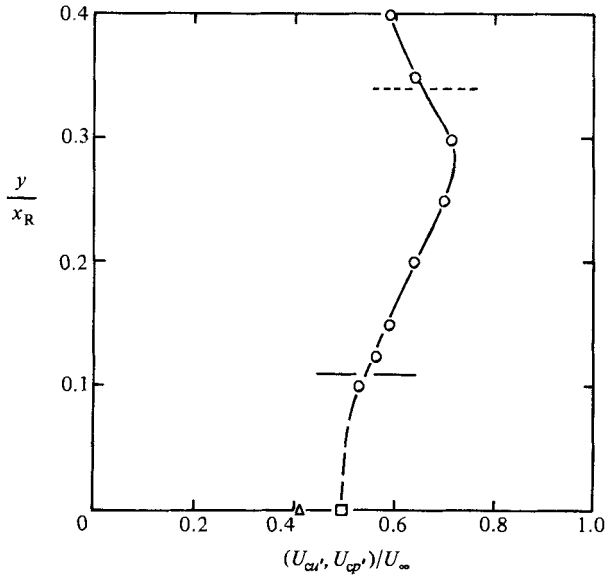

FIGURE 17. Distribution of phase velocities $U_{cu'}$ and $U_{cp'}$ in the reattachment section $x/x_R = 1.0$: ○, $U_{cu'}$; □, $U_{cp'}$; △, $U_{cp'}$ (Hillier & Cherry 1981*a*); ---, y_δ; ——, y_C (solid line for visual aid only).

and downstream of the reattaching zone. From the discrete-vortex simulation of KSA and also from Komatsu & Kobayashi's (1980) experiment, among others, the pressure fluctuation at a fixed position is found to be negative beneath large-scale vortices and positive when no such vortices exist above that position. The positive skewness implies that the pressure waveforms are positively spiky. The positive spikes are probably produced by the inrush of irrotational fluid of high total pressure towards the plate surface.

3.7. *Phase velocity and integral lengthscales of velocity and surface-pressure fluctuations*

Figure 17 shows the distribution of the phase velocity $U_{cu'}$ of u' in the reattachment section. Two single hot-wire probes were mounted on a traversing mechanism in such a way that they were always at the same height y/x_R from the plate surface. The longitudinal coordinate of one wire was $x/x_R = 0.8$, while that of the other was $x/x_R = 1.2$. The cross-correlation of u' at the two positions gave a time lag which was used to estimate the phase velocity in the reattachment section $x/x_R = 1.0$. The phase velocities are approximately between $0.5U_\infty$ and $0.7U_\infty$, attaining a maximum $0.7U_\infty$ at a height a little below the edge y_δ of the separation bubble.

The phase velocity $U_{cp'}$ of the surface-pressure fluctuation p' at a particular position x was obtained by measuring the time lag between the outputs of the two pressure transducers placed at $x \pm 0.2x_R$. The value of $U_{cp'}$ on the reattachment line is $0.5U_\infty$, and seems to be joined smoothly to $U_{cu'}$ (see figure 17).

Figure 18 shows the distributions (in the reattachment section) of the longitudinal integral lengthscale $L_{xu'} (= U_{cu'} T_{u'})$ and the spanwise lengthscale $L_{zu'}$ obtained from the cross-correlation of u' at two positions separated in the spanwise direction. The lengthscale $L_{xu'}$ remains nearly constant at $0.12x_R$ across the bubble, whereas the spanwise length $L_{zu'}$ increases significantly with increasing y. The latter suggests that,

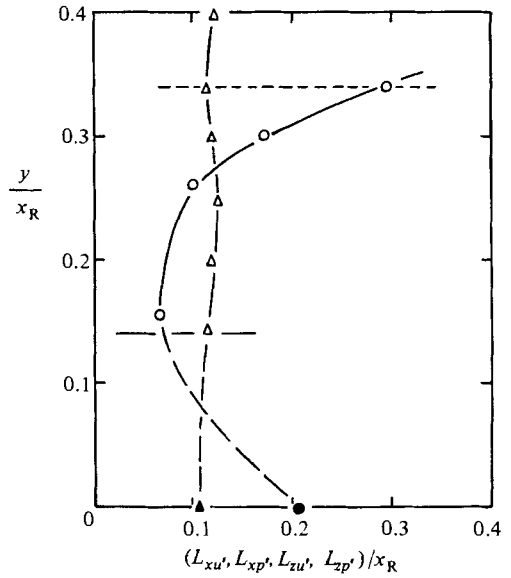

FIGURE 18. Longitudinal and spanwise integral lengthscales of longitudinal-velocity and surface-pressure fluctuations in the reattachment section $x/x_R = 1.0$: △, $L_{xu'}$; ▲, $L_{xp'}$; ○, $L_{zu'}$; ●, $L_{zp'}$ (Hillier & Cherry 1981*a*); ----, y_δ; ——, y_C (other lines for visual aid only).

in the central part of the bubble, coherent velocity fluctuations associated with large vortices are contaminated by small eddies which are highly three-dimensional. Such small eddies are expected to reduce the spanwise length $L_{zu'}$. The almost-constant longitudinal scale $L_{xu'}$ is conjectured to be brought about by a combined effect of the small eddies and the low-frequency flapping of the separated shear layer (see §3.8). A perusal of the autocorrelation of u' indicated that a drop of the correlation near zero time lag was greater at y_C than at y_δ. This can produce a shorter timescale $T_{u'}$ at y_C than at y_δ. On the other hand, the flapping manifested itself as a somewhat slower decay of the autocorrelation for large time lag at y_C than at y_δ. This is because the vertical velocity gradient $\partial U/\partial y$ is the greatest near y_C: the flapping is felt much more strongly at y_C than at y_δ. Such slow decay of the autocorrelation tends to increase the timescale $T_{u'}$. A combined effect of the small eddies and the flapping happened to be a slight increase of $T_{u'}$ as y decreases from y_δ to y_C (see figure 13). This increase of $T_{u'}$ is offset by a decrease of the phase velocity $U_{cu'}$ to produce almost constant lengthscale $L_{xu'}$ across the bubble.

The ratio $L_{zu'}/L_{xu'}$ is about 0.5 at the centre y_C and about 2.6 at the edge of the bubble. It may be noted that the value $L_{xu'}/x_R = 0.12$ on y_δ in the reattachment section is about 20% greater than that of the plane mixing layer, where x_R should be interpreted as the distance measured from the origin of mixing. The spanwise length of the surface-pressure fluctuations $L_{zp'}$ along the reattachment line is approximately equal to $L_{zu'}$ in the reattachment section.

The spanwise integral lengthscales $L_{zu'}$ along y_δ and y_C are plotted in figure 19 against the longitudinal distance. The lengthscales $L_{zu'}$ are fairly constant downstream of the reattachment line, as are the timescales of the velocity fluctuations (see figure 14). An increase of $L_{zu'}$ with increasing x up to the reattachment line is perhaps associated with the amalgamation of rolled-up vortices, which produces larger and larger vortices in the downstream direction. Vortices of larger cross-section are

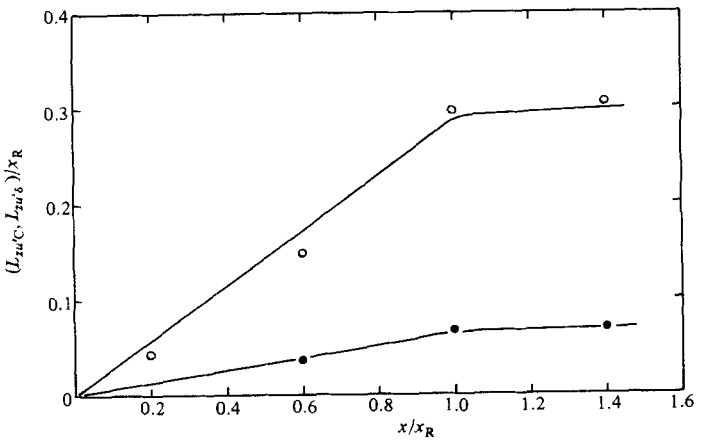

FIGURE 19. Spanwise integral lengthscales of u' along y_C and y_δ plotted against x/x_R: ○, $L_{zu'\delta}$; ●, $L_{zu'C}$ (solid lines for visual aid only).

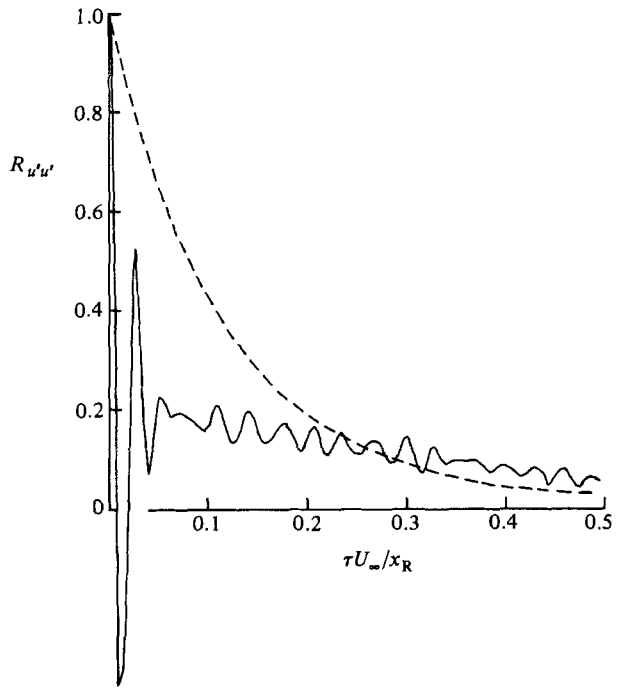

FIGURE 20. Autocorrelation of longitudinal-velocity fluctuations $R_{u'u'}$ near the centre of the separated shear layer: ——, $x/x_R = 0.02$; – – –, 0.4.

expected to yield velocity fluctuations that are more correlated in the spanwise direction.

3.8. *Flapping of the shear layer and large-scale unsteadiness in the bubble*

The autocorrelation coefficients of the longitudinal velocity fluctuation $R_{u'u'}$ near the centre of the shear layer y_C are shown in figure 20 for two positions shortly downstream of the separation line. The autocorrelations have a long tail which was clearly observed up to the section $x/x_R = 0.5$. Such a tail was gradually lowered as

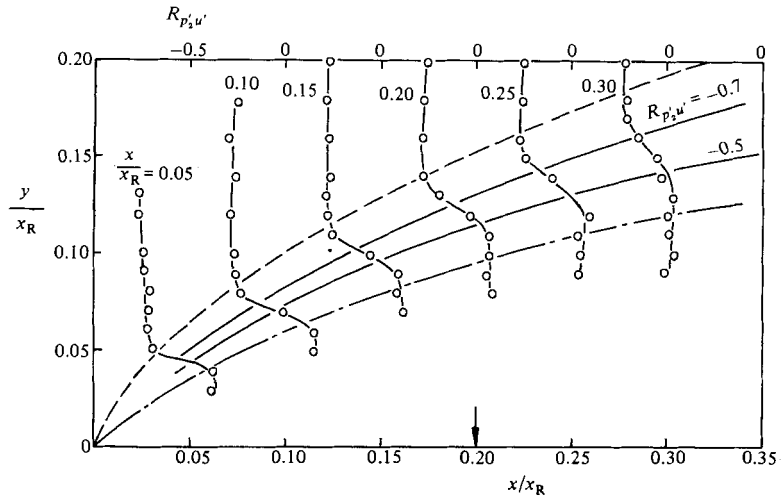

FIGURE 21. Cross-correlation of longitudinal-velocity and surface-pressure fluctuations. The signals were low-pass filtered ($0.25U_\infty/x_R = 50$ Hz) before processing. The vertical arrow ↓ shows the location of the fixed surface-pressure transducer whose output is denoted by p_2'. ———, y_C; - - - - -, y_δ (other lines for visual aid only).

x/x_R increased further, but a trace of the tail was still obvious even in the reattachment section. At $x/x_R = 0.02$, a high-frequency periodic wave is superposed on the tail, the non-dimensional frequency fx_R/U_∞ being approximately 30. This high-frequency component can be interpreted as the frequency at which the rolled-up vortices in the shear layer pass through the position of a fixed hot-wire probe. We assume that the tails of the autocorrelation curves are associated with the low-frequency flapping motion of the shear layer near the separation line. The flapping is probably produced by a large-scale unsteadiness in the bubble, the origin and nature of which are still unclear. The gradual decay of the tails in the more-downstream sections $x/x_R > 0.5$ may be explained by the cross-sectional dimensions of the rolled-up vortices, which are much larger than the spatial extent of the flapping of the shear layer. It is possible that the flapping can change the centre of the large vortices in the lateral direction, but the velocity fluctuations associated with such change of the vortex centre are weaker than or comparable to those caused by the vortex itself. This is conjectured to be the reason why the flapping is observed most clearly near the separation line, where the cross-sectional dimensions of the rolled-up vortices are at least comparable to the spatial extent of the flapping.

In order to get an idea about the spatial extent of the flapping, the cross-correlation between u' and p' was measured in the (x, y)-plane at many points in the upstream part of the separation bubble, the surface-pressure transducer being fixed at the position $x/x_R = 0.2$. Since the flapping frequency is estimated to be less than about $0.2U_\infty/x_R$, the velocity and pressure signals were passed through a low-pass filter ($0.25U_\infty/x_R = 50$ Hz) before being fed to the signal processor. The result is shown in figure 21. The cross-correlation is negative and the constant-correlation curves are approximately parallel to y_C. These features are conjectured to be further indirect evidences of the flapping motion. In particular, the fact that the cross-correlation is negative can be shown to be consistent with the flapping motion of the shear layer if the quasi-steady approach is employed. When the shear layer moves from its time-mean position towards the plate surface, the longitudinal velocity at the edge

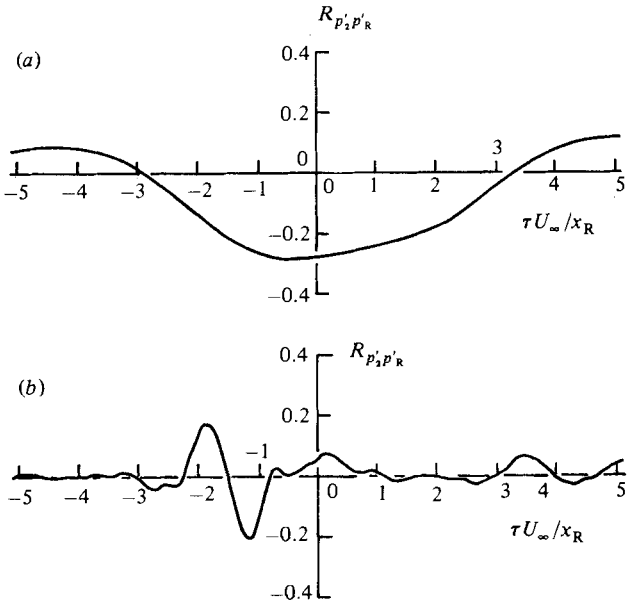

FIGURE 22. Cross-correlation of surface-pressure fluctuations at $x/x_R = 0.2$ and 1.0 (*a*) 50 Hz ($= 0.25U_\infty/x_R$) low-pass filtered; (*b*) 50 Hz high-pass filtered before processing. p'_2 and p'_R are pressure fluctuations at $x/x_R = 0.2$ and 1.0 respectively.

increases because of an increased curvature of the shear layer near the separation line. Since the pressure on the plate surface can be assumed to be approximately equal to the pressure at the edge of the shear layer, the surface pressure then becomes lower than the time-mean value. Thus we have $u' > 0$ and $p' < 0$. On the other hand, when the shear layer moves outwards from its time-mean position, a decrease in the curvature of the shear layer leads to $u' > 0$ and $p' < 0$.

The negative cross-correlation can be interpreted in another way. In the irrotational region the unsteady form of Bernoulli's equation yields

$$\overline{p'u'} = -\rho(U_\infty - U_c)\,\overline{u'^2},$$

where higher-order terms are neglected and U_c is a representative convection velocity of u' (Bradshaw 1967). If we assume with Bradshaw that the surface-pressure fluctuation did not differ markedly in character from the pressure fluctuation near the edge of the turbulent region, the above equation predicts negative cross-correlation between u' and the surface-pressure fluctuation. The result of figure 21 is consistent with this prediction. It should be emphasized, however, that the source of the fluctuations in this case is the flapping of the separated shear layer.

Figure 22 shows the cross-correlation of the surface-pressure fluctuations at two largely separated sections $x/x_R = 0.2$ and 1.0; the signals were low-pass filtered (50 Hz) before processing. The cross-correlation is negative over a wide range of the time lag. The phase $\phi_{p'_2p'_R}$ of the pressure fluctuations p'_2 and p'_R at $x/x_R = 0.2$ and 1.0 respectively are presented in figure 23, which shows that the phase is $-\pi$ in the frequency range $fx_R/U_\infty \leqslant 0.2$. This corresponds to the fact that p'_2 and p'_R are mostly of the opposite sign. A steplike change of the phase at $fx_R/U_\infty \approx 0.2$ may again indicate that the flapping of the shear layer occurs with frequencies less than about $fx_R/U_\infty \approx 0.2$. Moreover, the cross-correlations between u' at a fixed position

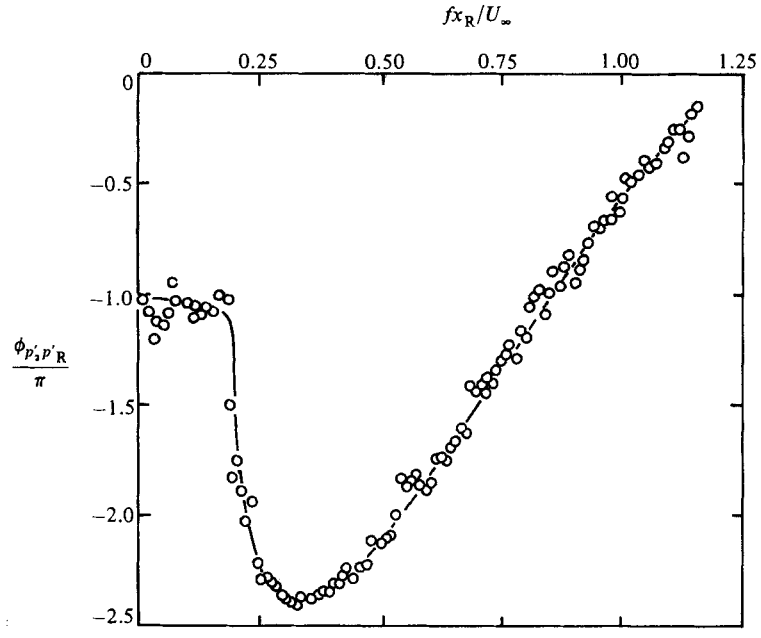

FIGURE 23. Phase of surface-pressure fluctuations p'_2 and p'_R at $x/x_R = 0.2$ and 1.0 respectively (solid line for visual aid only).

$(x/x_R = 0.2, y/x_R = 0.15)$ near the separation line and p' at various longitudinal positions were negative for $x/x_R \lesssim 0.6$ and positive for $0.6 \lesssim x/x_R \lesssim 1.2$.

These features suggest the existence of a large-scale unsteadiness in the separation bubble. As mentioned above, positive p' at the position $x/x_R = 0.2$ implies that the shear layer has moved outwards from its time-mean position. The negative cross-correlation shows that this is accompanied by negative p' at a distant position $x/x_R = 1.0$. On the other hand, the inward movement of the shear layer is accompanied by negative and positive p' at $x/x_R = 0.2$ and 1.0 respectively. Employing the quasi-steady approach, the position $x/x_R = 1.0$ can be said to be located upstream of the instantaneous reattachment line or within the instantaneous separation bubble when p' at the same position is negative. If this position is located downstream of the instantaneous reattachment line or outside the instantaneous separation bubble, then we expect positive p' at $x/x_R = 1.0$. Accordingly, the flapping of the shear layer is closely related to the shrinkage and enlargement of the separation bubble. It should be emphasized that this large-scale unsteadiness is different from the smaller-scale unsteadiness caused by the previously mentioned 'regular' vortex shedding from the bubble; the representative frequency of the former is much lower than that of the latter by a factor of roughly 6.

We imagine that very weak regular vortex shedding occurs from the main body of the separation bubble, and as a result a large amount of vorticity is accumulated within the bubble. This is accompanied by a considerable increase of the bubble length and the outward motion of the shear layer. When a sufficient amount of vorticity is accumulated, an extremely large vortex is eventually shed from the bubble; the bubble then rapidly shrinks and the shear layer moves inwards. The same feature has recently been observed in the discrete-vortex simulation of the separation bubble (see figure 24) and also in Hillier & Cherry's (1981*b*) smoke photograph (figure 2 of their paper).

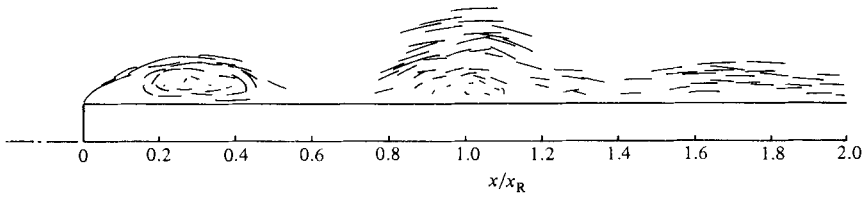

FIGURE 24. Shedding of an extremely large vortex from the separation bubble simulated by the discrete-vortex model (Kiya *et al.* 1982). Line segments show paths of elemental vortices during a short time interval.

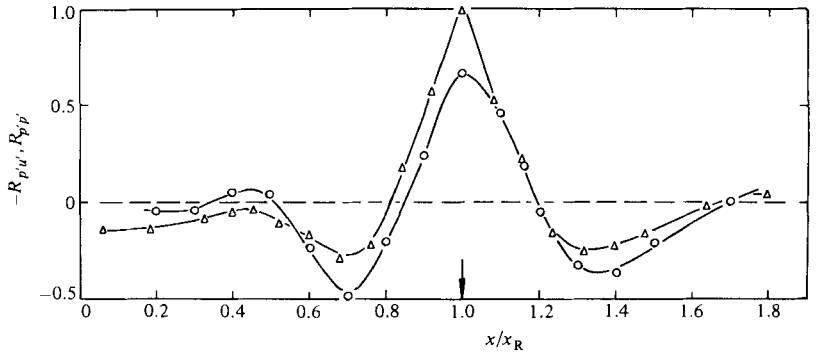

FIGURE 25. Cross-correlation of surface pressures $R_{p'p'}$ and that of surface pressure and longitudinal velocity $R_{p'u'}$: △, $R_{p'p'}$ (Hillier & Cherry 1981*a*); ○, $-R_{p'u'}$ (present result). The vertical arrow ↓ shows the longitudinal coordinate of the fixed pressure transducer and hot-wire probe. The y coordinate of the hot-wire probe is $y/x_R = 0.4$.

3.9. *Cross-correlations between surface-pressure and velocity fluctuations; further measurements*

The surface-pressure fluctuations beneath the separation bubble are closely related to the velocity fluctuations associated with the large-scale vortices existing above the surface. The cross-correlations between the surface-pressure and velocity fluctuations can thus give some aspects of the large-scale vortices in the separation bubble.

In order to show supporting evidence for this conjecture, figure 25 compares the cross-correlation between the pressure fluctuations at two positions separated in the longitudinal direction (Hillier & Cherry 1981*a*) with that between u' at a fixed point in the outer part of the bubble and the pressure fluctuations at various longitudinal positions. The x-coordinates of the fixed pressure transducer in the former case and the hot-wire probe in the latter were chosen as $x/x_R = 1.0$, the y-coordinate of the hot wire being y_B. Since $R_{p'u'}$ is negative when u' is taken in the outer part of the bubble (see figure 26), $-R_{p'u'}$ is presented in figure 25. The fact that the two correlation curves are fairly similar demonstrates that the correlation $R_{p'u'}$ can be used to find the large-scale vortex structure in the separation bubble, probably except the vicinity of the separation line where the rolled-up vortices are somewhat remote from the surface.

The profile of $R_{p'u'}$ gives an idea about an 'averaged' spatial waveform of the fluctuating surface pressure. The reasoning is as follows. When u' measured at the position (x_R, y_B) (temporarily denoted by u'_{BR}) is positive there exists a large vortex beneath y_B as demonstrated by KSA. At the same instant the surface-pressure

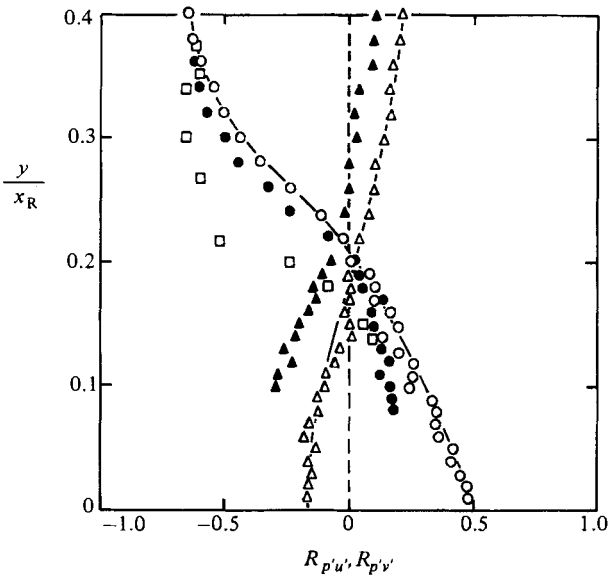

FIGURE 26. Cross-correlation coefficients of surface-pressure and velocity fluctuations measured at the reattachment section $x/x_R = 1.0$: ○, $R_{p'u'}$ (split-film result); ●, $R_{p'u'}$ (hot-wire result); □, $R_{p'u'}$ (Hillier & Cherry 1981*a*, hot-wire result); △, $R_{p'v'}$ (split-film result); ▲, $R_{p'v'}$ (hot-wire result) (solid lines for visual aid only).

fluctuation p' is negative at x_R. In the statistical sense, when u'_{BR} attains a maximum, it is reasonable to assume that the position (x_R, y_B) is just above the vortex centre, so that p' at x_R takes a negative minimum. p' is positive on both sides of the vortex, and thus a maximum of p' is expected to appear at the middle of two consecutive vortices. Accordingly the cross-correlation $R_{p'u'}$ between u'_{BR} and p' at various longitudinal positions takes a negative minimum when p' is measured beneath the vortex centre and a positive maximum when p' is taken at the middle of the two consecutive vortices. In this sense the cross-correlation $R_{p'u'}$ gives an information about the spatial waveform of the surface-pressure fluctuation, which is the average over a large number of realizations.

The correlation is negative beneath the position where u' is measured, and becomes positive on both sides of the negative region. The distance between the peak and valleys of $-R_{p'u'}$ indicates a rather large distance between the large-scale vortices. A typical distance is approximately $0.7x_R$, which is close to the distance $0{\cdot}8x_R$ evaluated from the phase velocity $U_{cp'}$ and the frequency $0.6U_\infty/x_R$ at which the vortices pass through a fixed position in the reattaching zone. Hillier & Cherry (1981*a*) also estimated the distance to be $0.6x_R$.

The cross-correlation $R_{p'u'}$ becomes positive when u' is measured in the lower part of the bubble as shown in figure 26. The fact that the correlation is negative in the outer part of the bubble can be explained in terms of the unsteady form of Bernoulli's equation: see the discussion of figure 21. The cross-correlation $R_{p'v'}$ between the surface-pressure and lateral-velocity fluctuations is also included in this figure. The signs of $R_{p'u'}$ and $R_{p'v'}$ are generally such that the Reynolds shear stress $-\rho\overline{u'v'}$ is positive.

We can construct from the correlations $R_{p'u'}$ and $R_{p'v'}$ a vector whose x- and y-components are the former and the latter respectively. The result is shown in figure 27, where the pressure transducer was fixed at $x/x_R = 1.0$ and the X-wire probe was

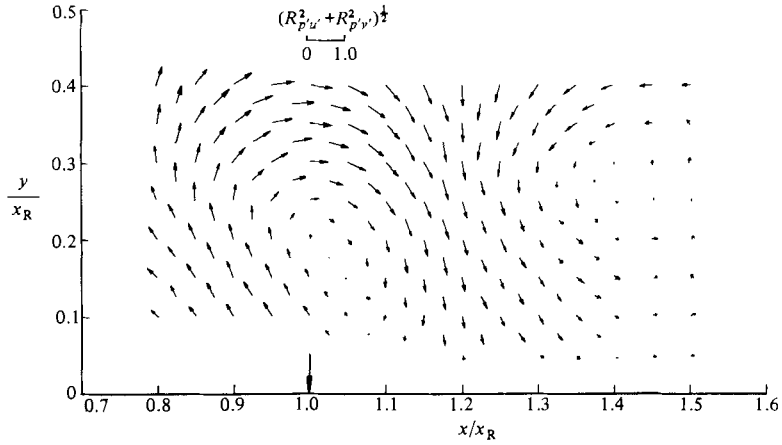

FIGURE 27. Vector fields of the cross-correlation coefficients $R_{p'u'}$ and $R_{p'v'}$. The x- and y-components of the vector are the former and latter respectively. Thick arrow shows the position of fixed pressure transducers, which is $x/x_R = 1.0$.

traversed in its vicinity. The vector fields can give an idea about an 'averaged' field of the velocity vector (u', v') in the large vortices by the same reasoning as explained before. The direction of arrows in figure 27 is arranged in such a way that the surface-pressure fluctuations are negative. The vector field suggests the existence of an inclined vortex rotating in the clockwise sense, whose downstream side is nearer to the surface than its upstream side. The same measurement was also made by fixing the pressure transducer at $x/x_R = 0.6$. A comparison between this result and figure 27 revealed that the height of the centre of the vortices and the longitudinal distance between them were a little larger in the downstream region than in the upstream region.

Figure 28 shows the loci of $R_{p'u'} = 0$ and $R_{p'v'} = 0$ in the reattaching zone. These loci can be interpreted as the lines on which the velocities u' and v' respectively are zero on the average. Tangents were drawn to the curves at the point of intersection, and ellipses of the same eccentricity were fitted in such a way that tangents to the ellipses at points of intersection between the former tangents and the ellipses were parallel to the x- and y-axes. In doing this, we assumed that the centre of the ellipses coincides with the vortex centre and that their axes are the bisectors of the first tangents. The centre of the ellipses may not exactly be the vortex centre owing to the effect of image reflection in the surface. This is not serious because we are interested only in a rough picture of the vortex. The resulting ellipses are included in figure 28. The major axis of the ellipses inclines by an angle of about 45° to the longitudinal direction, the minor radius being about 0.7 times the major radius.

Figure 29 shows the cross-spectrum, phase and coherence of the surface-pressure and velocity fluctuations in the reattachment section. The height of the hot wire from the surface was fixed at y_δ. The cross-spectrum and coherence have a somewhat broad but clear peak at a frequency near $fx_R/U_\infty = 0.6$. This frequency is again the frequency at which the large-scale vortices pass through the reattachment section.

3.10. *A three-dimensional aspect of the separation bubble*

The flow in the bubble has thus far been described from two-dimensional aspects. Since the surface-pressure fluctuations are well correlated with the large-scale

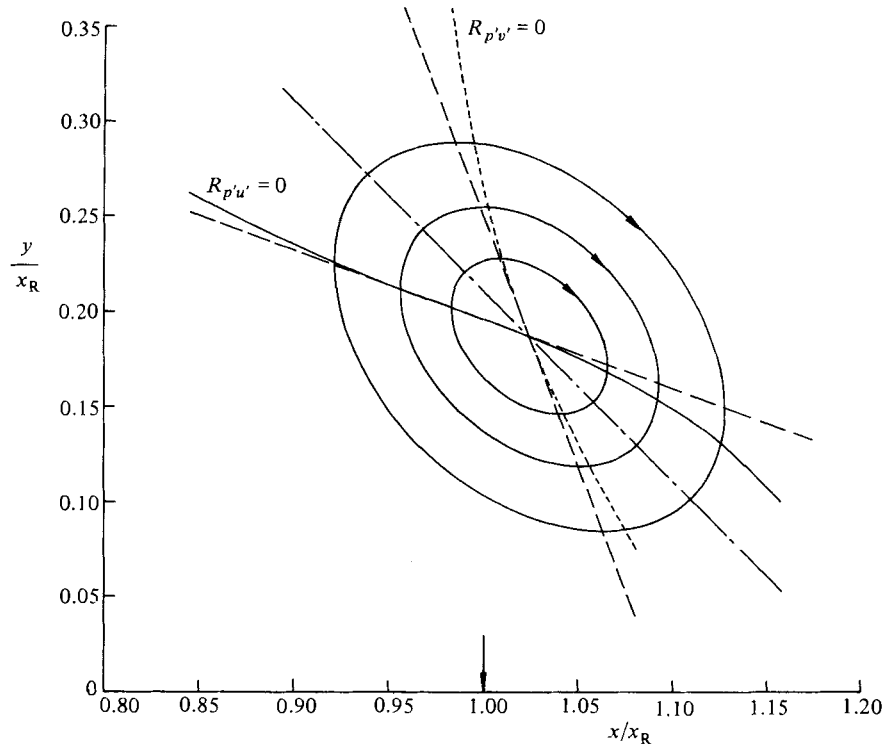

FIGURE 28. Qualitative picture of large-scale vortices in the reattaching zone. Ellipses give an idea about streamlines in the large-scale vortices. – – –, tangents to $R_{p'u'} = 0$ and $R_{p'v'} = 0$; — — —, bisector of the tangents (major axis of the ellipses). The vertical arrow ↓ shows the location of the pressure transducer.

vortices, it is expected that the cross-correlation coefficient $R_{p'w'}$ of the surface-pressure and transverse-velocity fluctuations can yield some information about three-dimensional features of the vortices in the separation bubble. Figure 30 shows the cross-correlation measured along several longitudinal lines in the plane $z/x_R = 0.35$. The pressure fluctuation was always taken at $x/x_R = 1.0$, and is thus denoted by p'_R in this figure. The distributions of the correlation along the corresponding lines in the opposite plane $z/x_R = -0.35$ were approximately antisymmetrical to those shown in figure 30. The sections $z/x_R = \pm 0.35$ were chosen because the correlation $R_{p'_R w'}$, which was measured along several spanwise lines in the reattaching zone by fixing the pressure transducer at the midspan, took a maximum or a minimum at $z/x_R = \pm 0.35$, such as shown in figure 31. The location where $R_{p'_R w'} = 0$ approximately falls on straight lines L_1 and L_2 which have an inclination of about 100° and 56° respectively with respect to the longitudinal direction. The loci L_1 and L_2 were also found when the same measurements were made in the plane $z/x_R = 0.25$ with the pressure transducer fixed at $x/x_R = 0.6$: the inclination was about 110° for L_1 and 83° for L_2. The sections $z/x_R = \pm 0.25$ were chosen by the same reason as for $z/x_R = \pm 0.35$.

The cross-correlation measurements were also made along three typical lines A, B and C (see figure 30) parallel to the z-axis. The three lines lie in a plane normal to the straight line L_2. The result is presented in figure 31. The correlation is almost zero

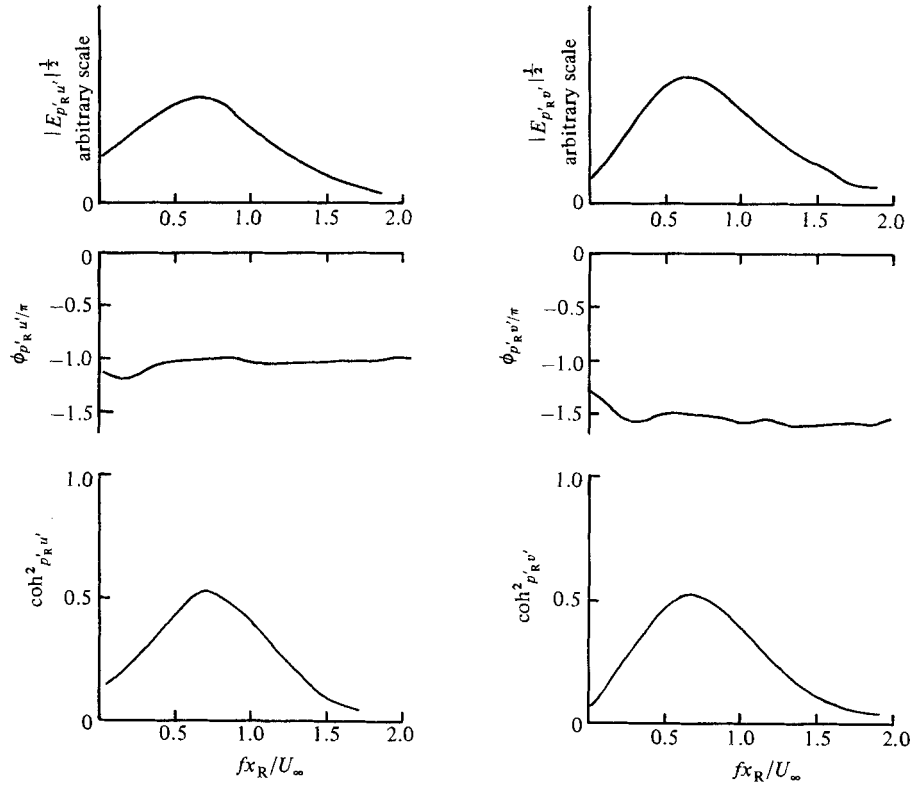

FIGURE 29. Cross-spectrum $|E_{p'_R u'}|$, $|E_{p'_R v'}|$, phase $\phi_{p'_R u'}$, $\phi_{p'_R v'}$ and coherence $\mathrm{coh}^2_{p'_R u'}$, $\mathrm{coh}^2_{p'_R v'}$ of surface pressure and velocity fluctuations in the reattachment section $x/x_R = 1.0$. The y-coordinate of the hot wire is y_δ. The vertical scales for $|E_{p'_R u'}|^{\frac{1}{2}}$ and $|E_{p'_R v'}|^{\frac{1}{2}}$ are linear but arbitrary.

along the line B but of the opposite sign along the lines A and C. Moreover, its distributions along A and C are approximately antisymmetrical with respect to the midspan. These features suggest the existence of a counter-rotating system shown in figure 31: the spanwise distance between centres of the system is estimated to be $0.6x_R$. The distance was roughly $0.5x_R$ when the surface-pressure fluctuation was measured at $x/x_R = 0.6$.

It should be mentioned that, since the aspect ratio of the separation bubble was $2.0x_R$ in this experiment, the distributions of the cross-correlation $R_{p'w'}$ were possibly affected by the sidewalls of the air tunnel. Nevertheless we conjecture that the general feature of its distributions is well represented by the present result.

At present we are unable to establish interrelations of the structure suggested by figures 30 and 31 and that of figures 27 and 28. Studies of the three-dimensional feature of large vortices in the separation bubble are now in progress in our laboratory by means of flow-visualization techniques and conditional-sampling measurements. A result is presented in figure 32, which is a flow-visualization photograph taken at a Reynolds number of 630 with an aspect ratio of 20. Fairly periodic spanwise structures are observed, at a Reynolds number lower, by two orders of magnitude, than that of the air-tunnel experiment. We suggest that the structures of large vortices do not differ markedly in character in the two cases. The spanwise distance

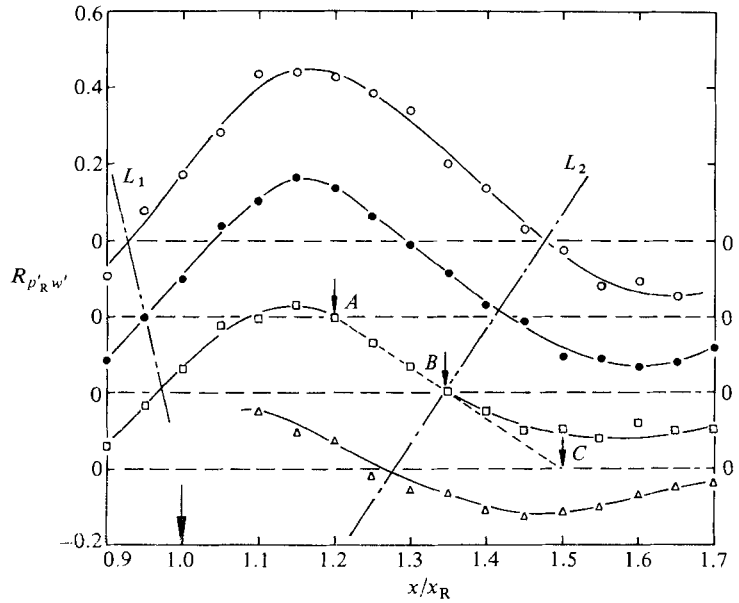

FIGURE 30. Cross-correlation between surface-pressure and transverse-velocity fluctuations measured in the plane $z/x_R = 0.35$ along several lines parallel to the x-axis. The surface pressure p'_R was measured at $x/x_R = 1.0$, as shown by the longest arrow. ○, $y/x_R = 0.4$; ●, 0.3; □, 0.2; △, 0.1. Coordinates of A, B, and C (denoted by short arrows) are $(x/x_R, y/x_R) = (1.20, 0.30)$, $(1.35, 0.20)$ and $(1.50, 0.10)$ respectively. ———, lines approximately passing through points of $R_{p'_R w'} = 0$.

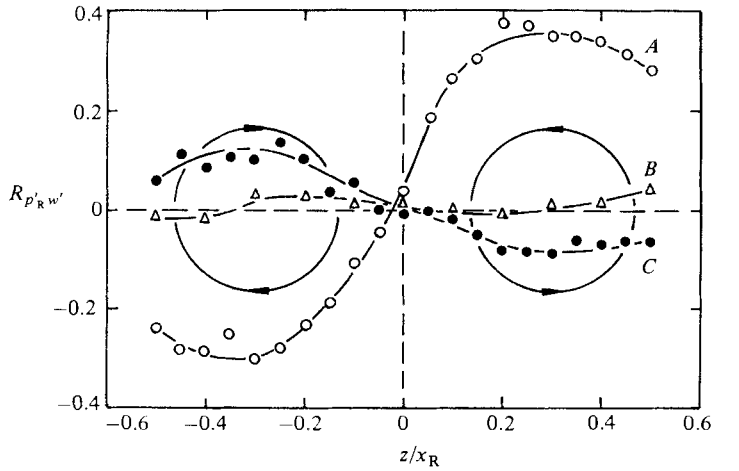

FIGURE 31. Cross-correlation between surface-pressure and transverse-velocity fluctuations measured along lines parallel to the z-axis which pass through the points A, B and C in figure 31: ○, A; △, B; ●, C. The circles are schematic representations of the structure in the plane which includes A, B and C, viewed from above. The direction of rotation corresponds to an instant when p'_R is negative.

between two neighbouring structures was roughly $0.7x_R$ in the reattaching zone when an average was taken for several similar photographs. This is close to the distance $0.6x_R$ estimated from figure 31. The phase coherence of the spanwise structure is perhaps lost in the air-tunnel experiment by the effects of freestream turbulence and noise in initial conditions at separation.

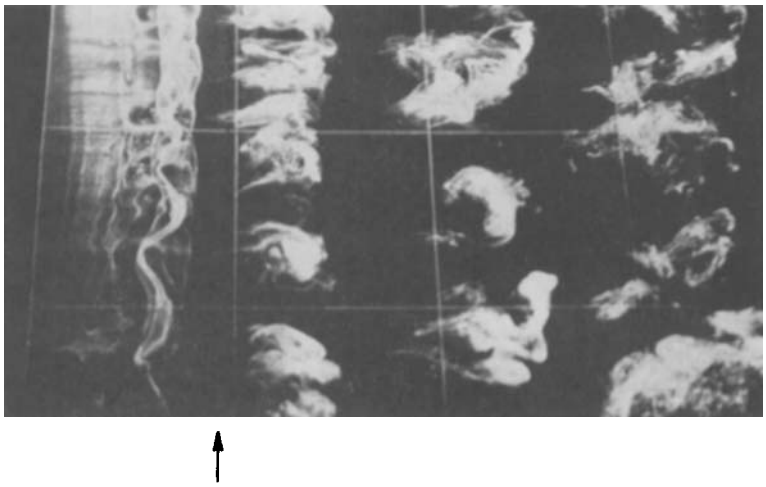

FIGURE 32. Photograph of the flow in the (x, z)-plane. Flow is from left to right. Visualization by hydrogen bubbles, which were produced by a thin platinum wire placed on the plate surface just downstream of the separation line. ↑, time-mean reattachment position; Reynolds number = 630; aspect ratio = 20.

4. Conclusions

The flow in the separation bubble formed along the sides of a blunt flat plate with right-angled corners has been described in terms of various statistical properties of the surface-pressure and velocity fluctuations.

Large-scale vortices are shed downstream from the separation bubble with a frequency of about $0.6U_\infty/x_R$. On top of this 'regular' vortex shedding, there exists a large-scale unsteadiness in the bubble; vortices much larger than the regular vortices are shed with frequencies less than about $0.2U_\infty/x_R$, the central frequency being about $0.12U_\infty/x_R$. The large-scale unsteadiness in the bubble is accompanied by a flapping motion of the shear layer near the separation line. The authors conjecture that the regular vortex shedding is hindered by still unknown mechanisms, and as a result a large amount of vorticity is accumulated within the bubble. This accumulation will lead to a large increase of the bubble length. The accumulated vorticity is eventually shed downstream as an extremely large vortex to suddenly reduce the bubble length to a great extent. The formation and shedding of such a large vortex are observed in Hillier & Cherry's (1981*b*) smoke photograph and also in the discrete-vortex simulation. The detailed nature of this large-scale unsteadiness in the bubble well deserves a further investigation.

The cross-correlations between the surface-pressure and velocity fluctuations were found to be useful means for the study of large-scale vortex structure in the bubble. This is because the vortices are strong enough to produce large pressure fluctuations, which can serve as a 'reference signal' to sort out the velocity fluctuations associated with the large-scale vortices. This situation in turn means that the velocity fluctuations at appropriate positions in the bubble can be used to obtain some information about the instantaneous distribution of the fluctuating surface pressure. The distance between the large-scale vortices estimated from such velocity–pressure cross-correlations is in fair agreement with the distance $0.8x_R$ evaluated from the phase velocity of the vortices and the frequency at which the vortices pass through a fixed position.

The spatial distributions of the cross-correlation coefficients $R_{p'u'}$ and $R_{p'v'}$ give an idea about the vortex structure in the reattaching zone, where the average centre of the vortices is estimated to be at about $0.2x_R$ from the surface and the average longitudinal distance between the vortices is $(0.7–0.8)\,x_R$. The loci on which $R_{p'u'}$ and $R_{p'v'}$ are zero can be interpreted as those on which u' and v' respectively are zero on the average. The position where they intersect can be taken as the vortex centre. By fitting ellipses of the same eccentricity to the loci, it was found that the major axis of the ellipses makes an angle of about 45° with the longitudinal direction in such a way that the downstream side of the ellipses is nearer to the plate surface than their upstream side. Moreover, the minor diameter of the ellipses is about 0.7 times the major diameter.

An aspect of the unsteadiness in the separation bubble was obtained in terms of the spatial distributions of the reverse-flow intermittency and the frequency of switching of the flow direction. The switching frequency is maximum along the line on which the reverse-flow intermittency takes the value of 0.5.

The approximately linear increase of the integral timescales along the edge of the separated shear layer indicates that the coalescence or amalgamation of rolled-up vortices occurs successively upstream of the reattaching zone. The timescales are almost constant downstream of the reattachment line; this suggests that the shed vortices travel downstream without significantly changing their structure within a certain distance after the reattachment.

The spanwise distributions of the cross-correlation between the surface-pressure and transverse-velocity fluctuations suggested the existence of a longitudinal counter-rotating system of fluid. The spanwise distance between the axes of the rotation is estimated to be roughly $0.6x_R$. The velocity fields conditionally averaged on the basis of the surface-pressure waveforms can produce more detailed flow structure in the separation bubble. Studies are now in progress and will be published in a forthcoming paper.

This work was financially supported by the Grant-in-Aid for Scientific Studies from the Ministry of Education, Science and Culture of Japan. We also thank Mr E. P. Sutton, Dr J. C. R. Hunt (University of Cambridge, United Kingdom), Mr H. Tamura and Dr Y. Suzuki for their valuable comments during the course of this work. We are grateful for referees' helpful comments.

REFERENCES

ANTONIA, R. A. & VAN ATTA, C. W. 1977 Statistical characteristics of Reynolds stresses in a turbulent boundary layer. *AIAA J.* **15**, 71–75.

BRADSHAW, P. 1967 Irrotational fluctuations near a turbulent boundary layer. *J. Fluid Mech.* **27**, 209–230.

BRADSHAW, P. & WONG, F. Y. F. 1972 The reattachment and relaxation of a turbulent shear layer. *J. Fluid Mech.* **52**, 113–135.

CHANDRSUDA, C. & BRADSHAW, P. 1981 Turbulence structure of a reattaching mixing layer. *J. Fluid Mech.* **110**, 171–194.

EATON, J. K. & JOHNSTON, J. P. 1982 Low frequency unsteadiness of a reattaching turbulent shear layer. In *Turbulent Shear Flows 3* (ed. L. J. S. Bradbury, F. Durst, B. E. Launder, F. W. Schmidt & J. H. Whitelaw), pp. 162–170. Springer.

FERNHOLZ, H. H. 1978 External flows. In *Turbulence*, 2nd edn (ed. P. Bradshaw), p. 45. Springer.

FIEDLER, H. & HEAD, M. R. 1966 Intermittency measurements in the turbulent boundary layer. *J. Fluid Mech.* **25**, 719–735.

HILLIER, R. & CHERRY, N. J. 1981*a* Pressure fluctuations under a turbulent shear layer. In *Proc. 3rd Turbulent Shear Flow Symp., Davis, California*, 9–11 September, pp. 16.23–16.28.

HILLIER, R. & CHERRY, N. J. 1981*b* The effects of stream turbulence on separation bubbles. *J. Wind Engng & Ind. Aerodyn.* **8**, 49–58.

JOHNSTON, J. P. 1978 Internal flows. In *Turbulence*, 2nd edn (ed. P. Bradshaw), p. 109. Springer.

KIYA, M., SASAKI, K. & ARIE, M. 1982 Discrete-vortex simulation of a turbulent separation bubble. *J. Fluid Mech.* **120**, 219–244.

KOMATSU, S. & KOBAYASHI, H. 1980 Vortex-induced oscillation of bluff cylinder. *J. Wind Engng & Ind. Aerodyn.* **6**, 335–362.

LANE, J. C. & LOEHRKE, R. I. 1980 Leading edge separation from a blunt plate at low Reynolds number. *Trans. ASME* I: *J. Fluids Engng* **102**, 494–496.

OTA, T., ASANO, Y. & OKAWA, J. 1981 Reattachment length and transition of the separated flow over blunt flat plates. *Bull. JSME* **24**, 941–947.

OTA, T. & ITASAKA, M. 1976 A separated and reattached flow over a blunt flat plate. *Trans. ASME* I: *J. Fluid Engng* **98**, 79–86.

OTA, T. & NARITA, M. 1978 Turbulence measurements in a separated and reattached flow over a blunt flat plate. *Trans. ASME* I: *J. Fluids Engng* **100**, 224–228.

WILLMARTH, W. W. & WOOLDRIDGE, C. E. 1963 Measurements of the correlation between the fluctuating velocities and the fluctuating wall pressure in a thick turbulent boundary layer. *AGARD Rep.* 456.

WOOD, D. H. & BRADSHAW, P. 1982 A turbulent mixing layer constrained by a solid surface. Part 1. Measurements before reaching the surface. *J. Fluid Mech.* **122**, 57–89.

WYGNANSKI, I. & FIEDLER, H. E. 1970 The two-dimensional mixing layer. *J. Fluid Mech.* **41**, 327–361.